Agricultural and Forest Meteorology 279 (2019) 107706

Contents lists available at ScienceDirect

Agricultural and Forest Meteorology

journal homepage: www.elsevier.com/locate/agrformet

Evaluation of modeled actual evapotranspiration estimates from a land surface, empirical and satellite-based models using *in situ* observations from a South African semi-arid savanna ecosystem

Floyd V. Khosa[a,b,*], Gregor T. Feig[a,c,d], Martina R. van der Merwe[a], Mohau J. Mateyisi[a], Azwitamisi E. Mudau[a], Michael J. Savage[b]

[a] Global Change and Ecosystems Dynamics, Natural Resources and Environment, Council for Scientific and Industrial Research, P.O. Box 395, Pretoria 0001, South Africa
[b] Agrometeorology Discipline, School of Agricultural, Earth and Environmental Sciences, University of KwaZulu-Natal, Pietermaritzburg, South Africa
[c] Department of Geography, Geoinformatics and Meteorology, University of Pretoria, Pretoria, South Africa
[d] South African Environmental Observation Network, PO Box 2600, Pretoria 0001, South Africa

ARTICLE INFO

Keywords:
Brutsaert–Strickler
CABLE
GLEAM
Granger–Gray
Szilagyi–Jozsa
Complementary relationship

ABSTRACT

Evapotranspiration (ET) plays a crucial role in the land-atmosphere interaction and climate variability, especially in arid and semi-arid areas. Accurate estimates of ET are important in hydrological and climate modeling. This study evaluates eight ET data products from different models used for ET estimation. The data products are classified into three main categories depending on the type of modeling approaches: namely process-based land surface model, empirical models, and satellite data derived estimates. The different model estimates are evaluated against *in situ* measurements from the Skukuza flux tower which is situated in a semi-arid savanna in South Africa. The correlation score and cantered root mean square error computed on monthly ET averages indicate that the satellite-derived model and land surface model estimates are closer to the observed ET signal for the Skukuza site, both in-phase and magnitude. The empirical models' outputs tend to reflect a relatively pronounced departure from observations in magnitude. The normalised mean bias computed for different seasons reveals that the estimates from all modeling approaches are close to the observed signal during the transition period (March–May) to the austral summer. In general, all models overestimate ET during summer and underestimate it in winter. A qualitative analysis of the year-to-year variation for different seasons reveals that all model estimates are qualitatively consistent with the observed seasonal pattern of the signal. Satellite and process-based land surface models (LSMs) also show a response to extremes events such as drought years. The study identifies satellite-derived model outputs as a candidate for understanding spatio-temporal variability of ET across different landscapes within the study region, and process-based models to potentially be used for climate change impact studies on ET.

1. Introduction

Evapotranspiration (ET), which is the transfer of water vapor to the atmosphere from the surface, plays a significant role in the modulation of global climate feedback, through its role in carbon, energy, and water cycles (Cao et al., 2010). Accurate estimates of the actual evapotranspiration (AET) are required for applications such as hydrological, climate and water resource modeling (Ding et al., 2013; Wang et al., 2010a; Xu and Chen, 2005). Studies for evaluating models for estimating AET, to be referred hereafter as ET, are generally are sparse. Such studies include the work done by Xu and Chen (2005), Xu and Singh (2005) and Zhang et al. (2016).

Many studies have evaluated the accuracy of the models for estimating potential evapotranspiration (PET), which is the amount of ET that would occur if the soil water supply was not limited (Bormann, 2011; Fisher et al., 2005; Lu et al., 2005; Shi et al., 2008), and reference (ET_o) or crop ET (Ahooghalandari et al., 2016; Cai et al., 2007; Pereira et al., 2015; Tabari et al., 2016; Valipour, 2014) which is ET from a reference surface, generally a specific crop type with certain characteristics with an unlimited water supply (Allen et al., 1998; McMahon et al., 2013). These models have been evaluated across different biomes (*e.g.*, forests, grassland and savanna), demonstrating that their performance is highly variable over space and time.

The methods for estimating ET have their inherent limitations

* Corresponding author at: Global Change and Ecosystems Dynamics, CSIR, Pretoria 0001, South Africa.
E-mail address: vkhosa@csir.co.za (F.V. Khosa).

https://doi.org/10.1016/j.agrformet.2019.107706
Received 11 December 2018; Received in revised form 27 July 2019; Accepted 13 August 2019
0168-1923/ © 2019 Published by Elsevier B.V.

associated with the fact that: (1) each method targets a specific temporal and spatial scale. In most cases, the spatial scale is larger than that covered by the localized *in situ* observations, (2) each of the estimation methods has specific assumptions, errors and technical challenges (Wilson et al., 2000). The limitations of various methods for estimating ET lead to the overall uncertainty in the values obtained. Bormann (2011) recommends that models (*e.g.*, atmospheric models coupled to LSM) be validated at a regional scale before they are applied for climate change studies. This is because comparisons between models and observation are generally problematic, particularly in the case where there is a mismatch in the spatial scale between modeled outputs and the point measurements. In the absence of spatially distributed *in situ* observations, point evaluation of various models is recommended (Haughton et al., 2018, 2016). In such cases, care needs to be taken to ensure that models are evaluated against observational sites that meet the uniformity assumptions about the drivers of the key feedbacks implemented in the models. To have confidence in these models, key land surface processes should be adequately simulated.

Three categories of models are evaluated in this study including land surface, empirical and satellite-based models. In particular, we evaluate two versions of the CSIRO Atmosphere Biosphere Land Exchange (CABLE-2.0 and 2.3.4) LSM, three commonly-used empirical models (Granger–Gray, Szilagyi–Jozsa, and Brustaert–Strickler) based on the complementary relationship and three versions of the Global Land Evaporation Amsterdam Model (GLEAM v3a, b, and c) satellite-based models. The models differ in their assumptions about drivers of ET, the forcing data and the implemented mathematical formulations for calculating ET. In LSMs for example, the schemes that control the transfer of water vapor from vegetated surfaces (*i.e.* transpiration) differ. This is an important component of the model concerning the simulation of ET, as transpiration from the canopy has been estimated to account for 60–80% of ET across the land surface (Jovanovic et al., 2015; Palmer et al., 2015). Empirical models differ in the mathematical structure and the satellite-based models differ in forcing data. Owing to the differences in the mathematical structure of the models, it is important to evaluate each of the models against observations, to investigate how they respond to the forcing data and how representative the models are for a specific region.

For South Africa, where a significant part of the total land area (32.5%) is covered by the savanna biome, much attention has been given to understanding the ability of remote sensing-based techniques to represent ET (Jovanovic et al., 2014; Majozi et al., 2017; Palmer et al., 2015; Ramoelo et al., 2014; Sun et al., 2012). Little attention has been given to the evaluation of process-based (*e.g.*, LSMs) estimates, particularly for the Savanna biome which is characterized by discontinuous tree cover and continuous grass cover (Ratnam et al., 2011; Whitley et al., 2017). There is a need for a detailed understanding of how process-based models represent ET per eco-hydrological zones within the region. However, such studies are constrained by a lack of ET measurements.

The limitations of ET measurements are not only confined to South Africa but affects large parts of the world. *In situ* ET measurements are a valuable source of information for evaluating and calibrating various models, as well as for understanding the response of different processes to ecological and climatic changes at various spatiotemporal scales. The main reason for the scarcity of ET measurements is that they are obtained through the use of sophisticated instrumentation, which is generally expensive and is not available for the majority of practical applications (Guo et al., 2016). Most of the measurement sites that are listed on the observational networks such as FLUXNET are temperate regions. The Skukuza site, which is used as a reference in this study, is located in a semi-arid savanna region and is the only South African measurement site that is listed on FLUXNET. The site provides a unique opportunity to evaluate ET models for the region.

In this paper, we work towards gaining an in-depth understanding of the patterns and representativity of the modeled datasets, by comparing them with *in situ* observations from a South African flux tower. To achieve this, we evaluate how the models perform in capturing the phase (*i.e.*, qualitative) and magnitude (*i.e.*, quantitative) of the observed ET from the Skukuza flux tower. In particular, we evaluate whether the differences between various model outputs and observations are significant or not. The differences are deemed insignificant if they are within the range of uncertainties in the observed ET fields, or the unpredictable internal variability of the observed fields. The study seeks to establish if the models can be used reliably to simulate local and regional ET conditions in Africa. For models that show an insignificant difference relative to observations, we discuss the spatial patterns for different biomes within the study region. In summary, the evaluation study aims to obtain an enhanced understanding of the outputs of the models relative to the flux tower observations and the potential mechanisms responsible for the identified differences in the performance of the models.

2. Materials and methods

2.1. Evapotranspiration models

2.1.1. Land surface model

The CSIRO Atmosphere Biosphere Land Exchange (CABLE) is a LSM used to calculate water, heat and carbon exchanges between the atmosphere and the land surface. The LSMs represent the land surface component of global climate models used to project climate (Abramowitz, 2005; Abramowitz et al., 2008; Kowalczyk et al., 2013). The CABLE model is suitable for use in climate models, and as a stand-alone (*i.e.* offline) model (Kowalczyk et al., 2006a,b; Law et al., 2012), however, it has not been explicitly tested against *in situ* observations from the African region. Based on the Penman–Monteith (P–M) equation, the model calculates the components of ET (*i.e.* canopy evaporation, plant transpiration, and soil evaporation). It takes into account soil moisture in addition to the standard meteorological variables used for estimating ET. The P–M equation is accurate in areas where vegetation is not water-stressed and the data for stomatal resistance (r_s) and net irradiance are available (Wang et al., 2010b). Soil evaporation (E_{sl}) from a wet surface is calculated using

$$\lambda E_{sl} = \Gamma(R_n - G) + (1 - \Gamma)\rho_a \lambda \delta q_d / r_s \tag{1}$$

where λ is the latent heat of vaporization (MJ kg^{-1}), $\Gamma = \Delta/(\Delta + \gamma)$, Δ the slope of the curve relating saturation water vapor pressure to air temperature (kPa °C^{-1}), γ the psychrometric constant (kPa °C^{-1}), ρ_a the air density (kg m^{-3}), δq_d the humidity deficit in the air (%), R_n the net irradiance (W m^{-2}) and G the ground heat flux (W m^{-2}). For a wet surface $E_{sl} = E_{sp}$, while for a dry surface $E_{sl} < E_{sp}$, where E_{sp} is the potential soil evaporation (mm). The actual E_s is estimated as a fraction, x of E_{sp} or E_{sl} given by;

$$\lambda E_s = x\lambda E_{sp} \quad \text{or} \quad \lambda E_s = x\lambda E_{sl} \tag{2}$$

Two variables are required to estimate E_s namely soil moisture and soil surface temperature (Kowalczyk et al., 2006a,b). Transpiration is estimated using:

$$\lambda E_t = \frac{\Delta R_n + c_p \rho_a D_a (G_{h,i} + G_{r,i})}{\Delta + \gamma (G_{h,i} + G_{r,i})/G_{w,i}} \tag{3}$$

where c_p is the specific heat capacity of air (J kg^{-1} °C^{-1}), D_a is vapor pressure density (kg m^{-3}), and $G_{w,\ i}$, $G_{h,\ i}$ and $G_{r,\ i}$ are the unit less conductance of water, heat, and radiation respectively. Evapotranspiration is then calculated as the sum of evaporation and transpiration (Kowalczyk et al., 2006a,b).

Two versions of the LSM are used in this study namely CABLE-2.0 and CABLE-2.3.4. The model is parameterized for a point (*i.e.*, Skukuza) and run offline. The motivation for running the model at a point is to capture ecosystem-scale properties. The model is forced with the site-specific meteorological data. The parameterization of the model entailed substituting default parameters with observed parameters at the site, the details of the parameterization are listed in Table A1 in the

Appendix). The distinguishing feature amongst the two model versions is the stomatal conductance schemes used. The stomatal conductance schemes are based on different theories namely the empirical and optimal approach. The empirical approach (*i.e.*, CABLE-2.3.4) is based on stomatal response to environmental factors (Medlyn et al., 2011). The optimal approach (CABLE-2.0) formulated by Cowan and Farquhar (1977) is based on a theory stating that stomata should minimize water loss, whilst maximizing carbon gain during photosynthesis. In CABLE-2.0, stomatal conductance (g_s, mol m^{-2} s^{-1}) is modeled following Leuning (1995):

$$g_s = g_0 + \frac{a_1 \beta A}{(C_s - \Gamma)\left(1 + \frac{D}{D_0}\right)} \tag{4}$$

where g_0 (mol m^{-2} s^{-1}), a_1 and D_0 (kPa) are fitted constants, A (μmol m^{-2} s^{-1}) is the assimilation rate (*i.e.* photosynthesis), C_s (μmol mol^{-1}) is the CO_2 concentration at the leaf surface, Γ (μmol mol^{-1}) is the CO_2 compensation point of photosynthesis, D (kPa) is the water vapor pressure deficit at the leaf surface, β is the empirical soil moisture stress factor computed as:

$$\beta = \frac{\theta - \theta_w}{\theta_{fc} - \theta_w};\ \beta[0, 1] \tag{5}$$

where θ (m^3 m^{-3}) is the mean volumetric moisture content in the root zone, θ_w (m^3 m^{-3}) is the wilting point and θ_{fc} (m^3 m^{-3}) is the field capacity. In CABLE-2.3.4, g_s is computed following Medlyn et al. (2011):

$$g_s = g_0 + 1.6\left(1 + \frac{g_1 \beta}{\sqrt{D}}\right)\frac{A}{C_s} \tag{6}$$

where g_1 is a fitted constant.

2.1.2. Empirical models

Three commonly used empirical models namely: Szilagyi–Jozsa (S–J), Brutsaert–Strickler (B–S) and Granger–Gray (G–G) models were evaluated in this study. These models use a complementary relationship to estimate areal AET. The complementary relationship is based on a hypothesis by Bouchet (1963) stating that PET and AET depend on each other in a complementary way, via feedbacks between the land and atmosphere for large and homogeneous areas, where there is little advective heat and moisture (Bouchet, 1963; McMahon et al., 2013). As the surface dries, the decrease in AET is accompanied by an equal but opposite change in PET. Therefore, the PET ranges from its value at saturation to twice this value (Xu and Chen, 2005; Xu and Singh, 2005). The three models differ in the formulas used to estimate wet environmental ET (ET_w), PET (ET_p), and AET (ET_a). The complementary relationship is represented by:

$$ET_a + ET_p = 2ET_w \tag{7}$$

In the advection aridity model (*i.e.*, B–S), ET_p is calculated by combining information from the energy budget and water vapor transfer in the Penman (1948) equation:

$$ET_p = \frac{\Delta}{\Delta + \gamma}\frac{R_n}{\lambda} + \frac{\gamma}{\Delta + \gamma}E_a \tag{8}$$

where E_a is the drying power of the air (mm day^{-1}):

$$E_a = f(U_z)(e_s - e_a) \tag{9}$$

where $f(U_z)$ is the function of mean wind speed U_z at a reference level z above the ground, e_a and e_s are the water vapor pressure of air and the saturation vapor pressure at the air temperature respectively. Furthermore, ET_w is calculated following Priestley and Taylor (1972) *i.e.*, $f(U_z) \approx f(U_2) = 2.626 + 1.381U_2$, partial equilibrium ET equation:

$$ET_w = \alpha\frac{\Delta}{\Delta + \gamma}\frac{R_n}{\lambda} \tag{10}$$

where α is the unit less Priestley–Taylor coefficient, $\alpha = 1.26$ is mainly cited in the literature. The B–S model estimates ET_a using:

$$ET_a^{BS} = (2\alpha - 1)\frac{\Delta}{\Delta + \gamma}\frac{R_n}{\lambda} - \frac{\gamma}{\Delta + \gamma}E_a \tag{11}$$

where ET_a^{BS} is the aerial ET (mm day^{-1}). The S–J model was originally developed by Szilagyi (2007) purely based on the complementary relationship (Eq. (7)), and further modified by Szilagyi and Jozsa (2008):

$$ET_a^{SJ} = 2ET_w - ET_p \tag{12}$$

where E_a^{SJ} is the ET (mm day^{-1}), in the S–J model ET_p estimated using the wind function proposed by Penman (1948). The G–G model estimates ET from un-saturated lands (McMahon et al., 2013), it was developed by Granger and Gray (1989) following the Penman (1948) equation:

$$ET_a^{GG} = \frac{\Delta G_g}{\Delta G_g + \gamma}\frac{R_n - G}{\lambda} + \frac{\gamma G_g}{\Delta G_g + \gamma}E_a \tag{13}$$

where E_a^{GG} is the ET (mm day^{-1}), G is the ground heat flux (MJ m^{-2} day^{-1}) and G_g is a dimensionless evaporation parameter based on various surface types, computed as the ratio of ET_a to ET_p:

$$G_g = \frac{ET_a}{ET_p} \tag{14}$$

The advantage of the empirical models is that they are easy to implement and they use standard atmospheric variables that are easily measured (Granger and Gray, 1989; Granger, 1998; McMahon et al., 2013). They are widely used because of their simplicity and practical applicability (Szilagyi, 2007). An understood artifact of the S–J and B–S models is that they occasionally estimate negative ET value for days with low net irradiance. The periods with negative ET values are not considered when computing evaluation metrics in this study. These models have been criticized in the literature for the uncertainty surrounding the α value and its physical significance (McMahon et al., 2013). The empirical models as described above are implemented in the "Evapotranspiration" package in the R programming software developed by Guo et al. (2016). These models were forced and parameterized (*e.g.* latitude, site elevation, and wind instrument height) specifically for the Skukuza site. These models represent the area covered by the flux tower footprint. The Universal constants used in the package are listed in Table A2 of the Appendix, and variables that are site-specific (*i.e.*, parameters) are listed in Table A3 of the Appendix. The EMP models are forced with the same datasets, with all the other settings being kept the same.

2.1.3. GLEAM v3

Global Land Evaporation Amsterdam Model (GLEAM v3.1) is a set of algorithms designed to estimate daily ET and its components from satellite data at a global resolution of 0.25°. The GLEAM model uses satellite-derived radiation, precipitation, air temperature, snow-water equivalent, soil moisture, vegetation cover fractions, soil properties, lightning frequency and vegetation optical depth (VOD) as input to derive ET. The Priestley and Taylor (P–T) equation is used to compute cover-dependent potential evaporation rate based on net irradiance and air temperature (Martens et al., 2017; Miralles et al., 2011):

$$\lambda E_p = \alpha\frac{\Delta}{\Delta + \gamma}(R_n - G) \tag{15}$$

where E_p is the potential evaporation rate (mm day^{-1}). The estimates of E_p are converted to ET and its components depending on the type of land cover. Land cover data is obtained from the MOD44B v51 satellite observations. ET is then calculated as:

$$ET = S \times ET_p + E_i \tag{16}$$

where E_i is the interception loss computed following Gash's model (Miralles et al., 2010), and S is the evaporation stress factor. The stress factor (S) for both short and tall vegetation is computed using:

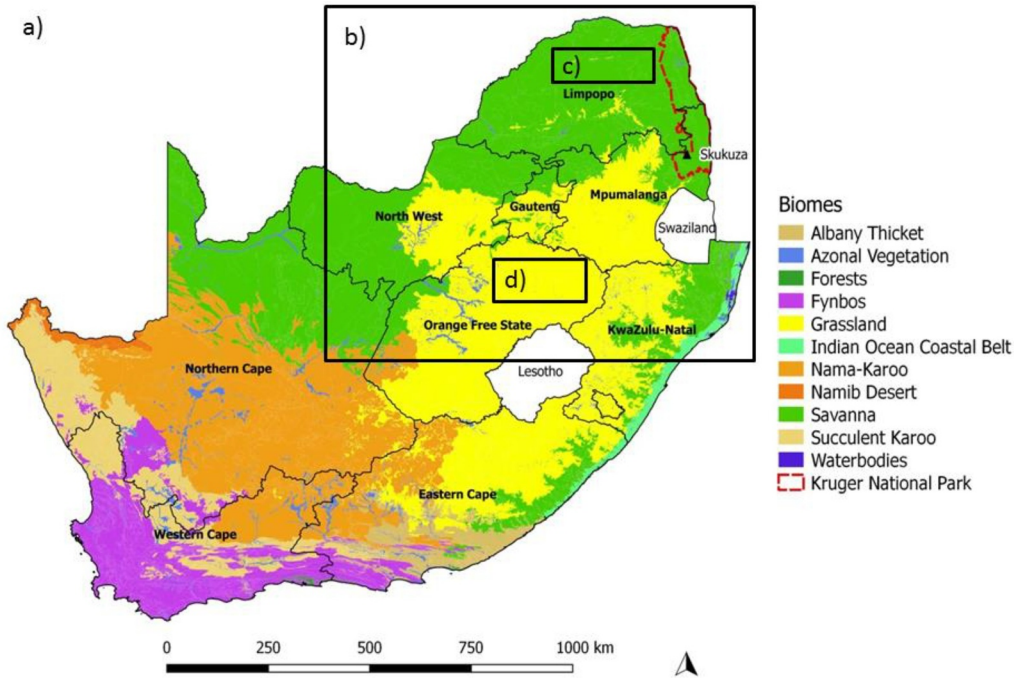

Fig. 1. (a) Map of South African biomes, Kruger National park and the location of the Skukuza flux tower. The biomes shapefiles for South Africa are downloaded from the South African national biodiversity institute (SANBI) website (http://bgis.sanbi.org/SpatialDataset), (b) the area considered for grid inter-comparison, (c) area used to represent the Savanna, and (d) grassland biome.

$$S = \sqrt{\frac{VOD}{VOD_{\max}}}\left(1 - \left(\frac{w_c - w^{(w)}}{w_c - w_{wp}}\right)^2\right) \tag{17}$$

where $VOD_{\max}$ is the maximum VOD for a specific pixel, w_c ($m^3\ m^{-3}$) is the critical soil moisture, w_{wp} ($m^3\ m^{-3}$) is the water retained below the wilting point and $w^{(w)}$($m^3\ m^{-3}$) is the soil moisture content of the wettest layer, assuming that water is drawn from layers in which it is more accessible by plants. For bare soil S is calculated as:

$$S = 1 - \frac{w_c - w^{(1)}}{w_c - w_r} \tag{18}$$

where $w^{(1)}$ ($m^3\ m^{-3}$) is the surface soil moisture and w_r ($m^3\ m^{-3}$) is the soil moisture that is not available for root uptake for bare soil (Martens et al., 2017). The P–T equation is used because it utilizes a few inputs, mainly those that are directly observed by satellites. Key features that differentiate this approach is the use of vegetation density, land surface temperature and microwave-derived soil moisture (Miralles et al., 2011). The strength of this model is that it produces spatially coherent estimates of water fluxes over land.

The GLEAM model has three versions, namely v3a, v3b and v3c. Version 3a uses satellite observed variables (soil moisture, radiation, reanalysis air temperature, snow-water equivalent, and vegetation optical depth) and a Multi-Source Weighted Ensemble Precipitation (MSWEP) dataset as inputs. This global dataset is from 1980 to 2016. Versions 3b and 3c use the same satellite input data, except soil moisture and vegetation optical depth which are based on measurements from different microwave sensors, namely European Space Agency Climate Change Initiative (ESA CCI) for v3b and Soil Moisture and Ocean Salinity (SMOS) for v3c. The periods of v3b and v3c are shorter, 2003–2015 and 2011–2015 respectively (Martens et al., 2017). A detailed description of the forcing data for the three GLEAM models is listed in Table A4 in the Appendix.

2.2. Data and evaluation site

The dataset used in this study to evaluate the models' performance is collected from the Skukuza flux tower collected through the eddy covariance method. The tower is located at an elevation of 370 m above sea level (25.0197°S, 31.4969°E) in the Kruger National Park (South Africa), a conservation area located in a semi-arid savanna ecosystem (Fig. 1). The Skukuza flux tower is the longest-running flux tower in South Africa and has been collecting data since August 2000 to date.

The flux tower site is located at a transition between two vegetation types, namely the broad-leaved *Combretum apiculatum* dominated savanna on the crests, which tend to have coarse sandy soil that is relatively nutrient-poor, and fine-leaved *Senengalia nigrescens* (*Acacia nigrescence*) savanna on sandy clay loam in the valleys, which is relatively nutrient-rich (Archibald et al., 2009; Feig et al., 2009; Scholes et al., 2001). The tower was deliberately placed on the ecotone of the vegetation types, to sample the different vegetation types (Scholes et al., 2001). There is a strong seasonal precipitation pattern with most of the rainfall occurring between November and April (Archibald et al., 2009). The grass layer is dominated by *Eragrostis rigidor, Panicum maximum*, and *Pogonarthria squarrosa* (Scholes et al., 2001). The woody vegetation at the Skukuza flux tower site is estimated to range between 8 and 10 m in height. The tower sensors are 17 m high with a fetch of approximately 500 m (Archibald et al., 2009). Therefore, the measurements do not only represent a point but a larger area (~500 m in diameter). The measurements are taken at 10 Hz and then averaged to half-hourly periods using the Eddy Pro software (Version 6.2.0). A description of the FT instruments used to collect the necessary input data for ET models are listed in Table A5.

The site data in this study is representative of about 0.2 km^2 (250 m radius) footprint as explained in Section 2.1. While the GLEAM model resolution is 25 km. The working assumption is that the time-averaged signal, from the observations and model outputs on time scales greater than a month is fairly developed, and stand a chance to show features reflective of the system as influenced by broader climatic patterns. Of course, this is a limited assumption but reliable within the neighboring region, with homogenous vegetation patterns across the biome and comparable climatic region forcings as is the case in this study. The comparison between modeled and measured data is only done for periods where there are no missing values in the observations. Furthermore, a comparison of the models is done at a point. Since the GLEAM models produce areal estimates of ET, data for a point where the Skukuza flux tower is located in the grid cell was extracted using the site coordinates nearest neighbor. This method is suitable as the data for the grid cell presents a spatial average ET value for the grid cell. The estimates by CABLE and empirical models are site (*i.e.*, point) specific. The datasets compared to measurements in this study are listed in Table 1. The lengths of the various ET datasets are not equal as shown in Table 1. The analysis is split into three by model type (*i.e.*, empirical

Table 1
Summary of datasets used.

Dataset	Data type	Period
In situ	Measurements	2001–2016
Brutsaert–Strickler	Empirical model	2001–2016
CABLE-2.0	Land surface model	2001–2011
CABLE-2.3.4	Land surface model	2001–2011
GLEAM v3a	Satellite-based model	1980–2016
GLEAM v3b	Satellite-based model	2003–2015
GLEAM v3c	Satellite-based model	2011–2015
Granger-Gray	Empirical model	2001–2016
Szilagyi-Jozsa	Empirical model	2001–2016

models, EMP; LSM and satellite-based models, SBM) as they differ either structurally or by forcing data.

2.2.1. Gap filling of input meteorological variables

The measured meteorological variables from the flux tower contain missing data mainly caused by equipment malfunction. The half-hourly data were converted to daily and used as input in the "Evapotranspiration" package in R. The ET package has internal gap-filling procedures for the inputs required to compute ET. Any gap-filling procedure results in biased estimates if the missing gaps exceed 20% (Enders, 2003). A study by Ukkola et al. (2017) to process FLUXNET data recommends that the threshold of missing data be between 15% and 20% per year. In this study, the threshold was set to a maximum of 20% per variable for the analysis period. The gap-filling procedures used in the package are adopted from Narapusetty et al. (2009). The percentage of missing values for the Rs exceeds 20% (Fig. A1). Therefore, the number of daily sunshine hours is used as an input instead (Guo et al., 2016). The number of sunshine hours is estimated following the method proposed by Abd el-wahed and Snyder (2015) using average daily air temperature. The flux tower data used as input in the empirical ET models are graphically shown in Fig. A1 in the Appendix. These include air temperature (Ta, °C), relative humidity (RH, %), incoming solar irradiance (Rs, W m^{-2}), wind speed (WS, m s^{-1}) and rainfall in mm day^{-1}. The meteorological forcing data for the CABLE model was gap filled with measured data from the nearest South African Weather Service (SAWS) station, located approximately 13 km away from the flux tower.

2.3. Model evaluation metrics

Regarding that, all models are limited to their assumptions about the drivers of ET. This study employs basic matrices that can potentially inform the fitness of the models for an envisaged purpose, and give insight on possible avenues for improvement. First, we look at the Taylor diagrams (Taylor, 2001) which graphically quantify the agreement between modeled data and observations by using the Pearson correlation coefficient (r) and the centered root mean square error (RMSE). In particular, the matrices are used to uncover whether there are significant differences between the modeled and observed signal for the site. We also calculate the normalised mean bias (NMB) to represent the degree of agreement between the observations and model outputs on a seasonal time scale. A time series plot for each season is presented to show the temporal variation of the modeled ET estimates against observations. The 80% data threshold is used to represent a month and season for both the *in situ* observations and model estimates.

3. Results and discussion

3.1. In situ evapotranspiration

As highlighted in the introduction, the main goal of this study is to evaluate models' performance in estimating ET against *in situ* data at the Skukuza semi-arid savanna site to assess the appropriateness of each of the modeling approaches to estimate ET from southern African ecosystems. Sixteen years (2001–2016) of measured ET data from the flux tower are used in this study (Fig. 3). The data are measured in the form of energy (*i.e.*, latent heat, LE) in W m^{-2} and converted to ET (mm day^{-1}) by dividing the observed LE by 28.94 (*i.e.*, 28.94 W m^{-2} is equivalent to 1 mm day^{-1}). The mean energy balance ratio (EBR) at the site computed at the 30 min temporal scale is 0.73, corresponding to a mean energy flux residual of 36.39 W m^{-2} over the period 2001–2016. The EBR is defined as the ratio between the sum of the turbulent convective and latent heat fluxes and radiation minus soil heat (Majozi et al., 2017). Details on the calculation of the EBR may be found in Högy et al. (2019). The daily processed time series data is displayed in Fig. 3. Ideally daily observed ET for the period would have 5844 (*i.e.*, N) data points. However, due to missing data only 3867 (*i.e.*, 66.17%) data points are available.

Fig. 2 shows the seasonal variation of ET at Skukuza, the amount of available and missing data (*i.e.* white cells), the inter-annual variation, and the range of ET using different color codes. The figure shows that in the following years 2002, 2006 and to a lesser extent 2015 had low data coverage.

ET is highest during the austral summer season (DJF), *i.e.*, hot and wet periods and low in winter (JJA), *i.e.*, cool and dry periods (Fig. 2). This is best reflected in the years with high data recovery. The ET temporal pattern is typical of a semi-arid savanna, where the water loss through ET is generally low (<1.5 mm day^{-1}). The summer of 2009 recorded the highest ET, with ET values ranging between 5 and 7 mm day^{-1}, in contrast, the summers of 2015 and 2016 recorded lower ET values. The period has been reported as the driest in more than 100 years in South Africa due to a "super" El Niño event (Oxford, 2017) and the ET measurements at Skukuza are reflective of that. The next section studies the sensitivity of ET at the site. This is done to identify the key variables that drive ET at Skukuza.

3.2. Sensitivity analysis of ET at Skukuza

One of the objectives of the paper is to obtain an in-depth understanding of the modeled and observed data sets for the site and evaluate the modeled outputs against the observations. A natural starting point is to discuss the sensitivity of the observed ET to the driving meteorological variables. It is well established that the principal factors that drive ET include meteorological variables (*e.g.*, solar radiation, precipitation, air temperature, humidity and wind speed), ground cover (*e.g.*, plant density, litter cover, root depth and stomatal conductance) including soil properties such as soil type and soil moisture (Allen et al., 1998; Brown, 2014; Valipour, 2014; Wang et al., 2010a; Zhang et al., 2001). For the Skukuza site, a multivariate regression analysis fitted on the stationary (*i.e.*, de-trended and de-seasonalised) *in situ* time series data (Fig. A2 of the Appendix) reveals that, 53% (*i.e.*, R^2) of the variation is explained by air temperature, relative humidity, wind speed, surface soil moisture, and incoming solar radiation. Surface soil moisture and relative humidity (RH) explains most of the variation of ET (*i.e.*, these variables have the highest beta coefficients). This is further elaborated by a strong correlation between ET, RH and surface soil moisture (Fig. A3 of the Appendix).

The rest of the variation (*i.e.*, 47%) of ET at the Skukuza may be explained by other variables such as vegetation and soil characteristics. For example, the leaf area index would account for much of the variation of ET following a wet period, as precipitation is intercepted by the plants. Root depth and plant type account for some of the variation in ET during the dry period as the water is extracted from deep soil layers (Bonan, 2008). Air temperature, wind speed, and incoming solar radiation generally have the same effect on ET, an increase in these variables generally results in an increase in ET. This is also elaborated by the regression coefficients of these variables (Fig. A2) having the same sign. The median values of surface soil moisture and RH for Skukuza are 7 and 62% respectively. The results presented here are consistent with the finding of Bonan (2008) stating that air temperature is the dominant driver in cold regions and soil moisture in arid regions.

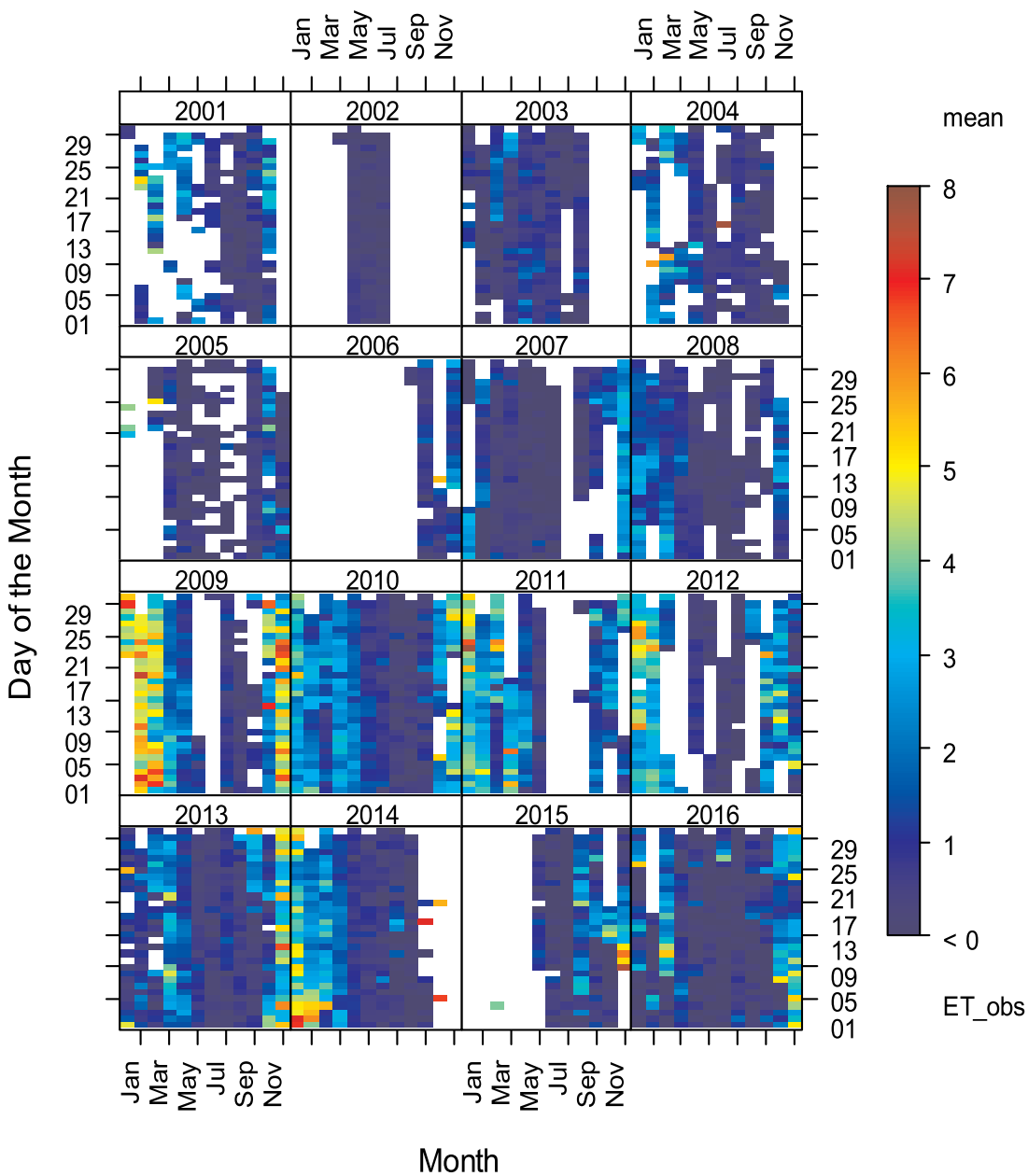

Fig. 2. Measured daily evapotranspiration (mm day^{-1}). The x-axis represents the month of measurement. The y-axis is the day of the month, and the *Z*-axis (color) represents measured ET (ET_obs). The dark blue color represents low ET measurements ranging between 0 and 2 mm day^{-1}. The dark red color represents high ET measurements between 6 and 8 mm day^{-1}. The white cells indicate missing data. (For interpretation of the references to color in this figure legend, the reader is referred to the web version of this article.)

3.3. Short-term seasonal comparison

A quantitative understanding of how the models compare against observations at inter-annual time scales can be gained by looking at the correlation coefficient (*i.e., r*), root mean squared error (*i.e.*, RMSE) and standard deviation. This is summarized through a Taylor plot Fig. 3. The GLEAM models (*i.e.*, SBM) have the highest correlation with the observations ranging between 0.6 and 0.8, showing that there is a strong positive relationship between the observations and GLEAM model outputs. The LSMs (*i.e.*, CABLE-2.0 and CABLE-2.3.4) data have the lowest correlation coefficients ranging between 0.4 and 0.5 (*i.e.*, moderate positive relationship) respectively, which are even lower than those between the empirical models (*i.e.*, EMP) and observations ranging between 0.5 and 0.6. The low correlation values between the CABLE simulations and observations are indicative that, there is a weak agreement in the phase of the inter-annual ET signal and the observations. This may be attributed to the bias in the forcing data which could have been introduced by the gap-filling of the input meteorological drivers.

The monthly *in situ* ET observations have a standard deviation of 31.94 mm month^{-1} shown by the black dotted line in Fig. 3. The GLEAM v3a model has a standard deviation of 31.42 mm month^{-1} which is close to that of the observations with a difference of 0.52 mm month^{-1}, CABLE-2.3.4 has a standard deviation of 32.84 mm month^{-1} indicating that the amplitudes of the observations and these models are similar. This means that these models capture the variability of the observed ET in magnitude. The standard deviations of GLEAM v3b, v3c and CABLE-2.0 are slightly higher than those of the observations ranging between 33.91 mm month^{-1} and 34.64 mm month^{-1} indicating a tendency towards slight overestimation of the observed ET by these models. The B–S and S–J models have far higher standard deviations almost twice that of the

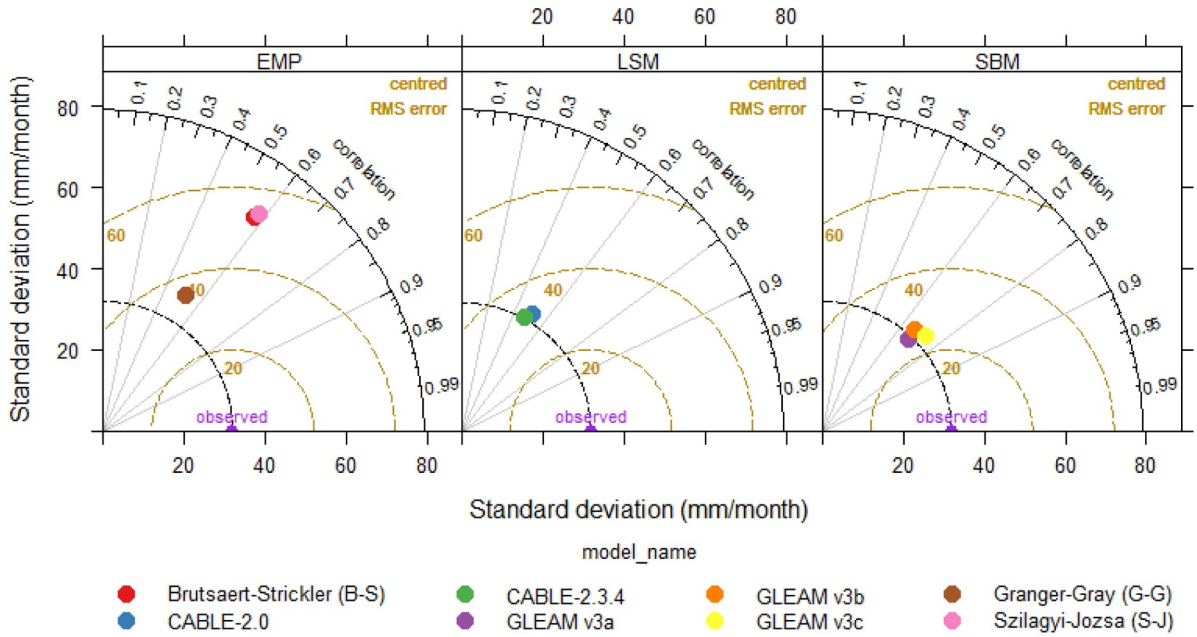

Fig. 3. Taylor Diagram comparing monthly modeled ET from empirical models (EMP), land surface models (LSM) and satellite-based models (SBM) with *in situ* observations. The dotted black line represents the standard deviation (mm month^{-1}) of the observations. The dotted caramel lines represent the centered root mean square error (RMSE) and gray vertical lines indicate the values of the correlation coefficients.

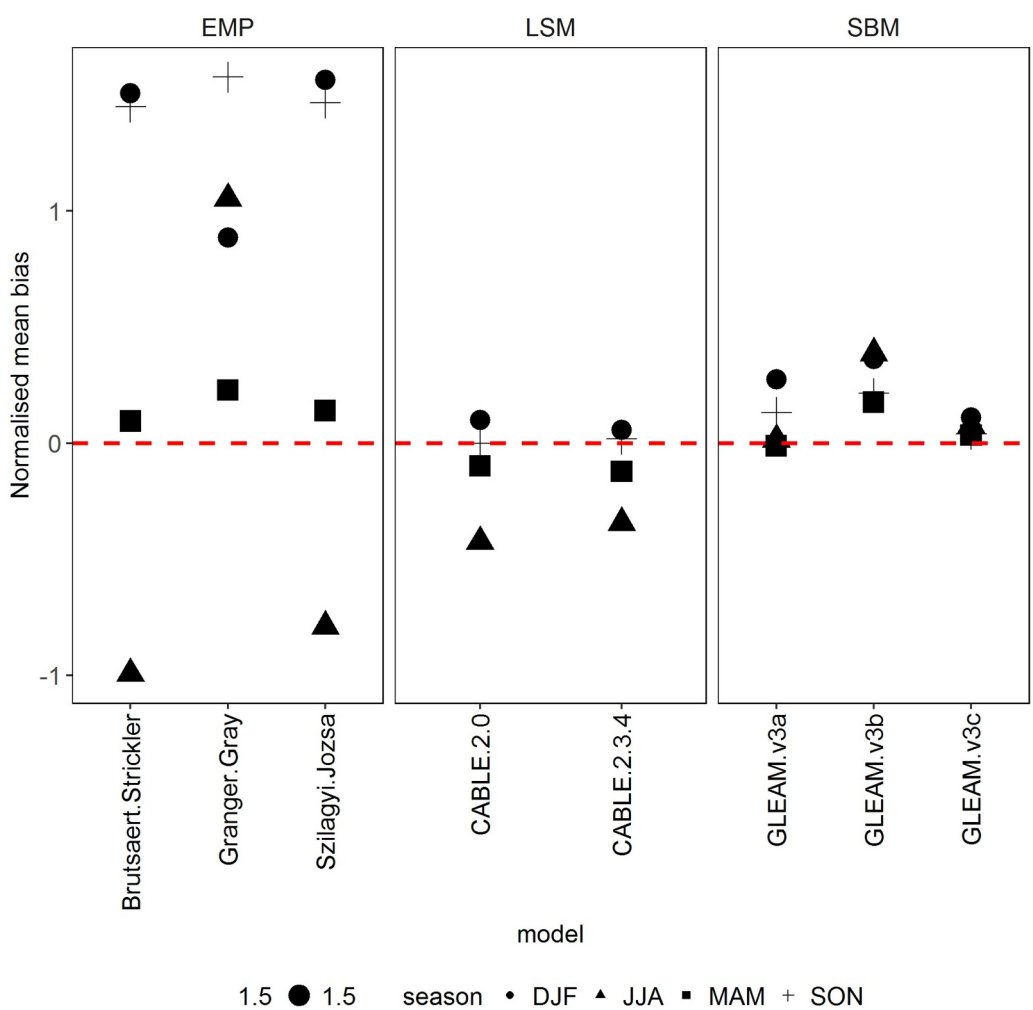

Fig. 4. The normalized mean bias (NMB) computed between the observations and the empirical models (EMP), land surface model (LSM) and the satellite-based models (SBM) across various seasons, namely; summer (DJF), autumn (MAM), winter (JJA) and spring (SON).

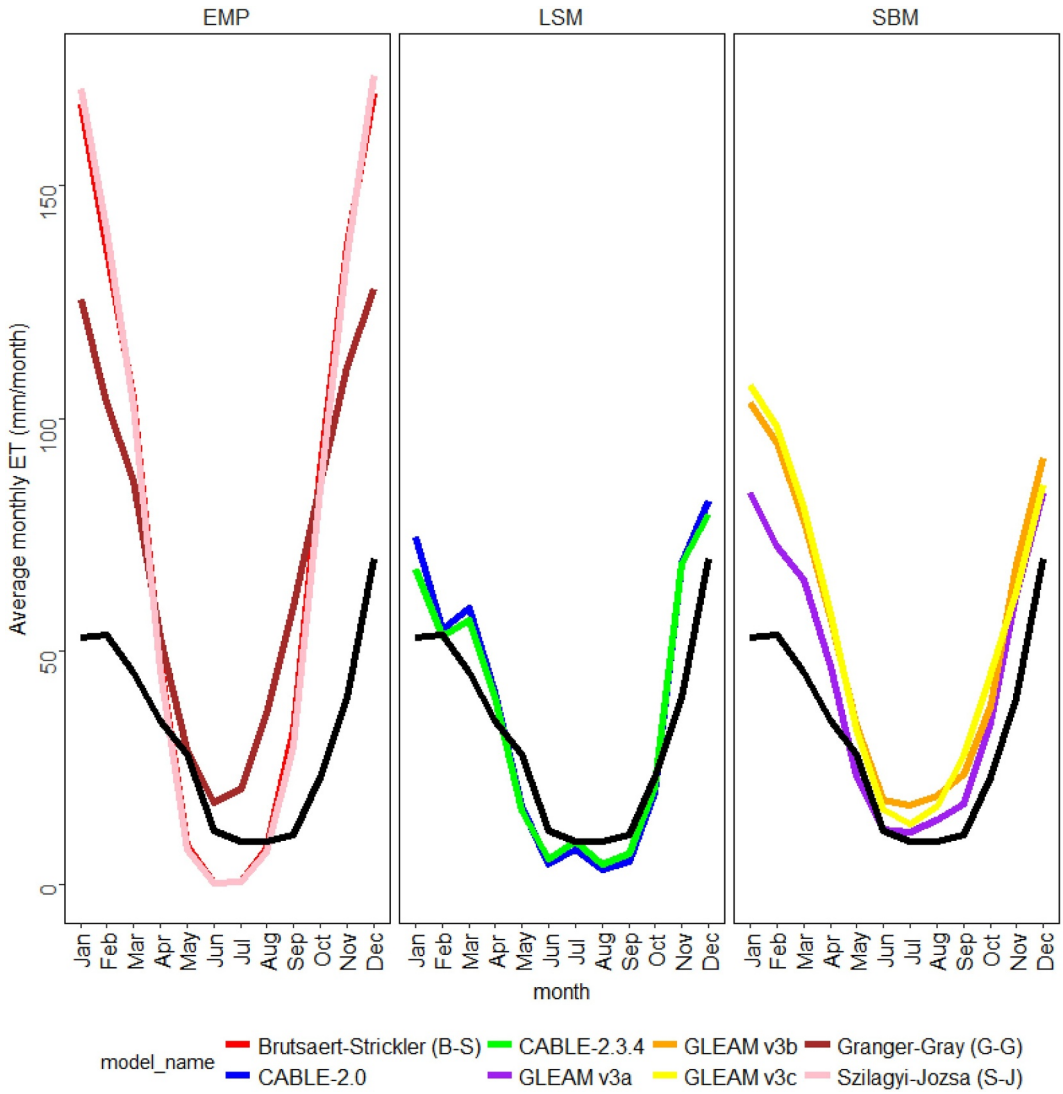

Fig. 5. Seasonal comparison of the long term monthly averaged modeled ET from empirical models (EMP), land surface models (LSM) and satellite-based models (SBM) with *in situ* observations (black).

observations (*i.e.*, more than 60 mm month^{-1}) indicating an overestimation of the observed monthly ET by these models.

As shown in Fig. 3, the GLEAM v3a, v3c, CABLE-2.0, and CABLE-2.3.4 have lowest RMSEs, 27.55, 28.91, 32.78 and 32.80 mm month^{-1} respectively. This is indicative that ET outputs for these models are not significantly different from that of observations in magnitude. This finding is also consistent with the discussion of the standard deviation values described above. In conclusion, we have learned that the EMP models generally overestimate the magnitude of observed ET. However, these models capture the observed monthly cycles of ET. The LSM generally captures both the phase and magnitude of the observed ET. The SBMs captures the monthly patterns of the observed ET with a slight overestimation of the magnitude especially by the v3b and v3c model variants.

From the Taylor diagram in Fig. 3, we learn that the degree of agreement in magnitude between the observation and model outputs is generally low. This is depicted by the RMSE which lies between (30 and 40 mm month^{-1}) for LSM, (20 and 30 mm months^{-1}) SBM and (35 and 58 mm month^{-1}) EMP. In Fig. 4 we unpack the nature of the agreement in magnitude by looking at the normalised mean bias (NMB) for the models for the four seasons (depicted in Fig. 4 by different shapes). The analysis has the potential to yield insight on the performance of the models in capturing the observed ET magnitude for the respective seasons. An obvious feature of the plot is that the LSM and SBMs have a relatively lower bias for the austral autumn season (MAM). The NMB for autumn ranges between −0.09 and 0.22 for all the models. The LSM and SBMs generally show the least bias on ET across all the seasons, with GLEAM v3a and v3c showing a strikingly low bias ranging between 0.03 and 0.27 in winter and between 0.01 and 0.07 in summer respectively. The LSM versions also show relatively low ET biases in spring of about −0.09. The EMP models, on the contrary, tend to either significantly overestimate or underestimate ET across the most seasons except for the spring season in which case the EMP models show a relatively low bias.

The P–M schemes in the LSM are considered to be the most robust and more physically realistic formulation of ET (Bonan, 2008). Their performance-based on magnitudes is reflective that their performance has a certain level of systematic uncertainty. We further observed that the performance of the two versions of the LSM is in general similar albeit with slight improvements in ET simulation of CABLE-2.3.4 relative to that CABLE-2.0. We can conclude that the use of the new stomatal conductance scheme (CABLE-2.3.4) did not result in major changes of ET simulation relative to the old scheme (CABLE-2.0). This finding is consistent with that report by De Kauwe et al. (2015).

3.4. Long-term seasonal comparison

In Fig. 5 we can see that both the observation and model estimates

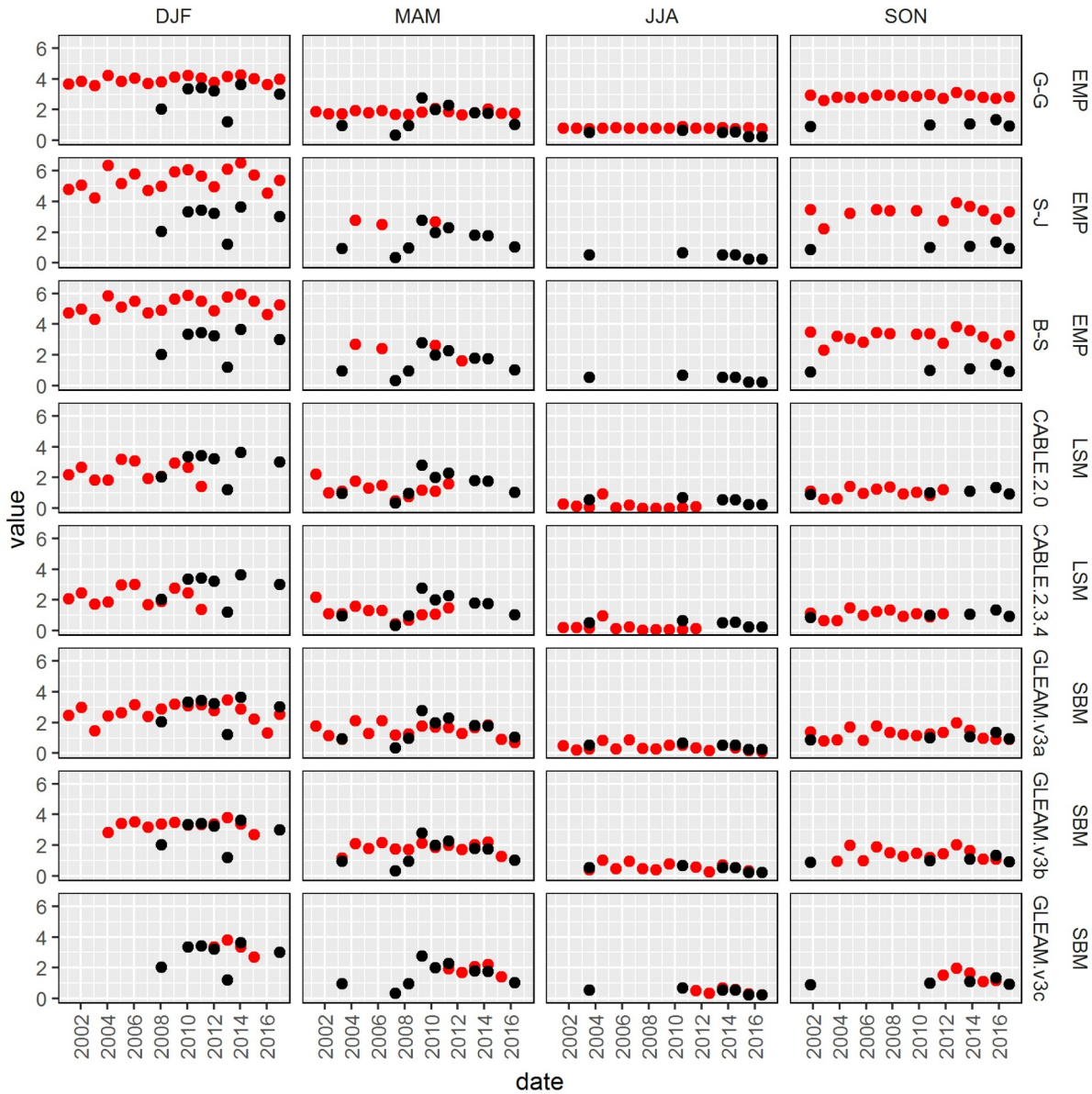

Fig. 6. Modeled (red) seasonal ET annually using the empirical models (EMP), land surface model (LSM) and satellite-based models (SBM) compared with *in situ* observations (black) at Skukuza. (For interpretation of the references to color in this figure legend, the reader is referred to the web version of this article.)

agree that ET is high during summer when it is hot and wet and low in winter when it is dry and cool. The elevated ET in summer is because there is sufficient energy to convert the abundant moisture, which is associated with high summer precipitation for the region into vapor (Allen et al., 1998). The seasonal cycles as presented by the empirical models (*i.e.*, EMP) is shifted relative to that of observations (Fig. 5). Particularly for those presented by the B–S and S–J models during the dry period (*i.e.*, winter). The two models show the dry months (*i.e.*, months of low ET) to be between May and August (3 months), while the observations show the dry months to be between June and September (3 months). The G–G empirical model underestimates the length of the dry period relative to the observations, which is between May and July (2 months). This is reflected by the low agreement in-phase ($r = 0.5$).

Both versions of the CABLE model capture the qualitative long term feature of the observed ET signal. As seen on the model bias results, there are slight differences between CABLE-2.3.4 and CABLE-2.0 which are most likely attributable to the improvements implemented in the stomatal conductance scheme used in CABLE-2.3.4. A study conducted by Zhang et al. (2016) concluded the CABLE model performed remarkably well in simulating monthly ET in cold (or polar) climates and predicted that it would perform well in arid and semi-arid regions. The long term pattern of ET confirms that the CABLE model adequately simulates the qualitative feature of the ET signal in a semi-arid South African site.

The satellite-based models (*i.e.*, GLEAM) generally capture the seasonal observed patterns. However, there is a noticeable departure of GLEAM output from observations during summer. The GLEAM v3a in comparison to versions 3b and 3c best captures the magnitude and phase of the observed ET. A long-term averaged ET signal may mask some features of the signal that occur at inter-annual time scales such as the influence of the El Niño-Southern Oscillation (ENSO) conditions on the ET signal. Therefore, it is instructive to evaluate the ability of the models to respond to such extreme meteorological events by looking at the ET signal at annual time scales.

3.5. Inter-annual comparison

In Fig. 6, the seasonal ET signal for the analysis period (*i.e.*, 2001–2016) is depicted for all the models and observations. An interesting question to ask is whether the models can capture the observed ET responses during anomalous years. In particular, we investigate if the models show sensitivity

to either wetter or drier years. We learn from Fig. 6 that the LSM and SBMs are consistent in capturing the year to year variations in ET across the seasons. In the autumn of 2009, the highest ET is observed, this is particularly reflected by GLEAM v3b. The LSM and SBMs show a lower ET in agreement with the observations for the austral winter (JJA) and spring (SON) during the year 2004. The year was reported to be a drought year (Masih et al., 2014). A similar low ET estimates in agreement with observation for the spring and winter seasons during the year 2007 can be seen. The period 2015/2016 was recorded as one of the driest periods on record (Oxford, 2017; Swemmer et al., 2018), this is also reflected by the observed ET and is captured by the SBMs. Unfortunately, it is not possible to match the model responses for all-season during anomalous years due to the data gaps, however, during the years of persistent drought, both LSMs and SBMs agree with the *in situ* observations in reflecting the ET pattern qualitatively. This gives confidence in the ability of the models to respond to the forcing data in calculating the temporal variations of ET. The EMP models largely overestimate (DJF and SON) and in some instances underestimate (JJA) the observed ET across the various years and seasons. The G–G model shows an almost uniform ET across the years and seasons relative to the observations that fluctuate across the years. A natural question to ask is whether the portrayed sensitivity for the LSMs and SBMs at a point scale can translate to a regional scale. An answer to this question is limited by the scarcity of observations spatially. However, it is still interesting to understand the seasonal nature of the model outputs at larger spatial scales. This will be discussed in Section 4.

Some of the observed differences between modeled and observed ET patterns across the three model types (*i.e.*, EMP, LSM, and SBM) can be associated with the differences in the assumptions about the drivers of ET and the models' response to the forcing data. The adequate performance by the SBMs and LSM relative to the EMP can be largely attributed to their robustness in their ET calculations. These models take into account more physical variables for estimating ET which are not considered by the simple EMP models. These include, for example, variables such as soil moisture, soil texture, vegetation types, and leaf area index. The SBMs use similar forcing data except for GLEAM v3a, which uses the MSWEP precipitation data making its performance slightly different compared to GLEAM v3b and v3c (Martens et al., 2017).

The EMP models use the same forcing data, however, they reveal a strong sensitivity to small changes in the free parameter (α) value concerning the estimation of ET. This was investigated in this study by varying the α value between 0.23 (default), 0.5 and 1. For this experiment, all the other variables were kept unchanged only varying the α value between 0 and 1 (restricted in the package). The results are presented in Fig. A4 showing highly variable ET estimates for the various EMP models. The issues surrounding the α value for these models have been also reported in the literature in a study by McMahon et al. (2013). We also learn that the (B–S and S–J) systematically produce negative ET values during the days of low radiation. Clearly, some of the bias in the EMP models emanate from how they respond to the forcing data for regions beyond which they were focused during their development.

4. Regional comparison of ET

Most of the evaluation indices reflect that the LSM and SBMs are capable of capturing the qualitative features of the ET signal, at least for months or seasons when the observed records were above the 80% data availability threshold. These models, therefore, present an opportunity for understanding the spatial variations, both in the quantitative and qualitative sense, across the landscapes of interest (Fig. 1b). A quantitative understanding of the seasonal patterns of ET can potentially inform an understanding of the water budget for applications at a regional scale. In this section, we present the results of the LSM and SBMs models at a resolution of 25 km. In the case of the LSM, default parameterization for variables such as vegetation classes is used. This is a departure from the point (*i.e.*, Skukuza site) where a highly detailed parameterization (described in Table A1 in the appendix) has been used. In the case of regional simulation vegetation and soil, parameters are represented by the dominant soil and vegetation types in each grid cell.

We learn in Fig. 7 that the SBM and LSM are qualitatively consistent with the observed seasonal spatial pattern of ET at the flux tower (shown in Fig. 2) for most of the savanna regions of South Africa. In those regions, ET is reflected as high in summer and low in winter. The reflected spatial pattern of ET makes intuitive sense from the knowledge of climate types for the regions (Kottek et al., 2006). This suggests that the two families of

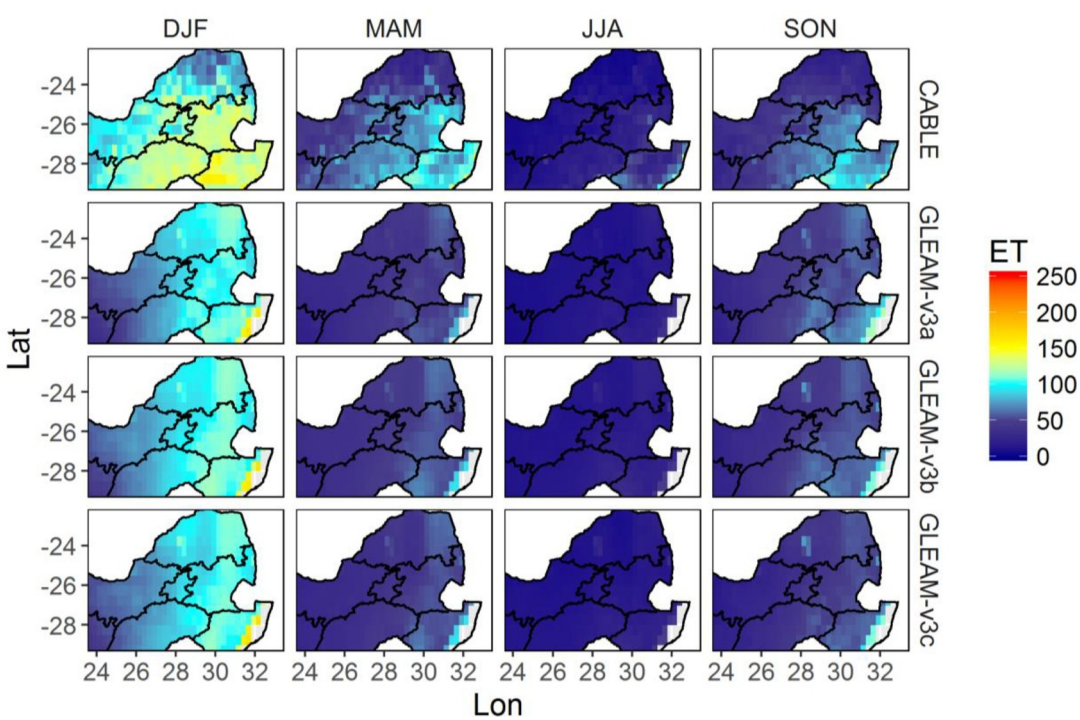

Fig. 7. Seasonal variability in ET across the region (Fig. 1b) dominated by the savanna and grassland biomes.

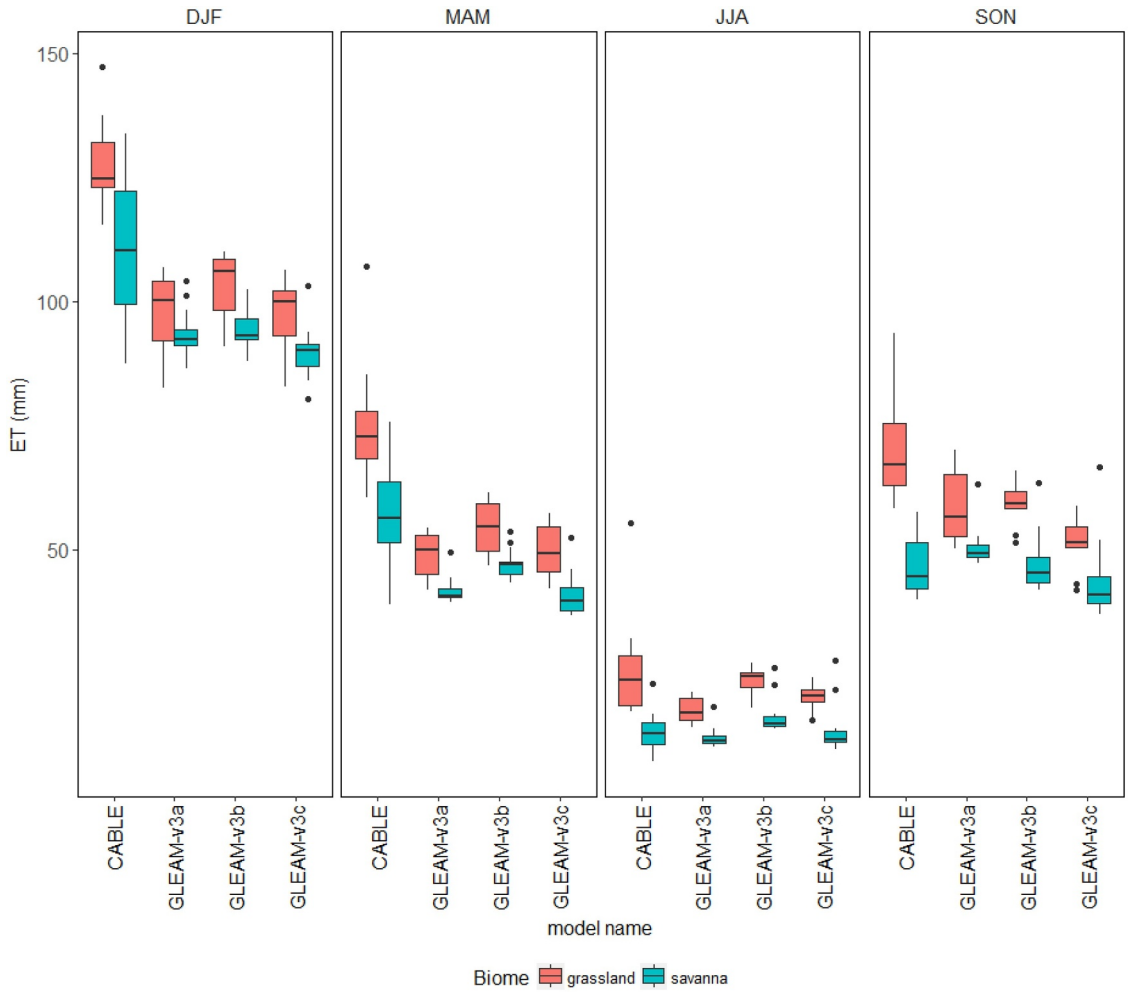

Fig. 8. Seasonal variability of monthly ET across the models and biomes. The data used here is extracted from two grid boxes dominated with the savanna (Fig. 1c) and grassland (Fig. 1d) biomes respectively.

models consistently translate the input data for calculating ET. In the absence of spatially distributed *in situ* observations, it not possible to conclude on which model has superior skill in estimating ET across the various landscapes. The CABLE model, for example, presents higher ET estimates in the grassland biome compared to the GLEAM models during summer. For the northern parts of Limpopo (savanna biome), the CABLE model presents lower values of ET ranging between 0 and 50 mm, compared to GLEAM models with ET values ranging between 75 and 100 mm. Despite these noticeable quantitative differences, it is encouraging to see that the consistency of the qualitative seasonal features of the signal observed at a point translates to broader landscapes. Most likely, the quantitative agreement between LSM and SBMs can be improved by fine-tuning the default parameter settings to better reflect the local conditions. This can be done for example by introducing local soil and vegetation parameters as opposed to using the default settings. The spatial pattern of ET presented in Fig. 7 is consistent with those presented by Jovanovic et al. (2015) using the MODIS satellite product. All these approaches suggest that ET in the eastern part of the study region is generally higher compared to the western parts where it is generally low. The box-and-whisker plots (Fig. 8) demonstrate the consistency in the responsiveness of LSM and SBMs to the seasonal changes in ET for the two dominant biomes within the study region, namely the savanna (Fig. 1c) and grassland (Fig. 1d).

5. Conclusions

The main aim of this study was to evaluate if the empirical (EMP), land surface (LSM) and satellite-based (SBM) models, for estimating ET were able to capture the observed ET at a South African semi-arid savanna site. The models evaluated differed either by model structure or forcing data. The three EMP models differed in the mathematical structure, two versions of a LSM differed in the stomatal conductance schemes, and the SMBs differed in the forcing data. The evaluation was conducted at monthly and seasonal temporal scales. The analysis was initiated by investigating the sensitivity of ET to various meteorological variables at the study site using multivariate regression. The analysis revealed that ET at the Skukuza site is most sensitive to soil moisture and relative humidity.

From the model evaluation results, we have learned based on the evaluation metrics (*i.e.*, correlation coefficient, root mean square error, standard deviation, and normalised mean bias) that, the empirical models generally overestimate the magnitude of the observed ET during summer, and underestimate ET during winter. However, the EMP models proved to be capable of capturing the phase of the observed monthly cycles. The two versions of the LSM generally captured both the qualitative (phase) and quantitative (magnitude) features of the observed ET signal. Based on the evaluation metrics, we have also learned that the use of the different stomatal conductance schemes in the model did not result in major changes in the simulation of ET. However, the use of the recent stomatal conductance scheme (version 2.3.4) resulted in slight improvements of the ET estimates. Similarly, the SBMs also capture the qualitative and quantitative features of the observed ET signal. The performance of the three versions of the SBMs is generally similar, with version 3a showing better agreement with the observations relative to the other version. This is attributed to the precipitation forcing data used for this particular model. Furthermore,

both the LSM and SBMs have shown to be able to capture the observed ET even during anomalous years, such as those that experienced drought.

The adequate performance by the SBMs and LSM relative to the EMP can be largely attributed to their robustness in their ET calculations. These models take into account more physical variables when estimating ET which are not considered by the simple EMP models. The poor performance of the EMP models is linked to uncertainties surrounding the alpha value, and them occasionally estimating negative ET values during the days of low radiation.

In the absence of spatially distributed data, we investigated whether the portrayed sensitivity for the LSMs and SBMs at a point scale can translate to a regional scale. These models displayed spatial consistent patterns at a regional scale across South African vegetation types. However, the LSM showed higher ET values across the region compared to the SBMs. This shows that a detailed parameterization of the LSM to represent key variables (*e.g.*, vegetation and soil types) representative of the region is necessary as was done at the site level before it can be used for climate change studies under various emission scenarios, future research may focus on this aspect. The study identifies satellite-derived model outputs as a candidate for understanding spatio-temporal variability of ET across different landscapes within the study region, and process-based models to potentially be used for climate change impact studies on ET. Future research may also focus on evaluating these models at multiple sites within different African biomes and savanna types.

Declaration of Competing Interest

The authors declare no conflict of interest. The funder had no role in the design, analysis, and interpretation of the data of this study.

Acknowledgments

We acknowledge Ms Humbelani Thenga's inputs on the flux tower data. We acknowledge Dr. Oscar Mokotedi for reviewing the manuscript.

Funding

This work was supported by the Council for Scientific and Industrial Research [project number EEGC030].

Supplementary materials

Supplementary material associated with this article can be found, in the online version, at doi:10.1016/j.agrformet.2019.107706.

Appendix

This Appendix consists of supporting information for this study. Section A.1 displays the sensitivity of ET measurements at the Skukuza site to meteorological variables. Section A.2 shows the parameterization of the CABLE model for the Skukuza site. Variables and constants that can be changed and those fixed in the evapotranspiration package used to estimate evapotranspiration using the empirical models are shown in Section A.3. forcing data for the three versions of GLEAM models are shown in Section A.4. Section A.5 discusses symbols and variable used in the study, and Section A.6 shows the results of the empirical models to the alpha value.

A.1. CABLE parameterization

Table A.1.

Table A1
Parameterisation of the CABLE model at the Skukuza site.

Parameter	Description	Units	Default	Site specific
bch	Parameter in Campbell's equation	–	4.2	4.2
Betaroot	Beta parameter to calculate froot	–	0.961	0.95
clay	Fraction of soil which is clay	–	0.09	0.172
css	Soil specific heat capacity	$J\,kg^{-1}\,K^{-1}$	850	850
Frac4	Fraction of C4 plants	–	0	0.6
hyds	Hydraulic conductivity at saturation	$m\,s^{-1}$	0.000166	0.000166
LAImax	Maximum leaf area index	$m^2\,m^{-2}$	MODIS climatological average leaf area index 1°x 1° grid	2.5
Leafangle	Leaf angle	°	0.25	0.25
leaflength	Leaf length	m	0.950	0.05
leafwidth	Leaf width	m	0.8	0.05
poolleaf	Mass of organic matter in the leaf pool	$kg\,m^{-2}$	300	245
poolwood	Mass of organic matter in the wood pool	$kg\,m^{-2}$	12,000	1000
rholeaf	Leaf reflectance	–	0.092	0.092
rholeafnir		–	0.380	0.39
rhosoil	Soil bulk density	$kg\,m^{-3}$	1600	1300
rhosoilvegnir		–	0.1	0.1
rhowood		–	0.16	0.16
rhowoodnir		–	0.39	0.39
rootveg		–	1029	192
Rp20	Plant respiration scalar	–	2.2	2.2
Rs20	Soil respiration scalar	–	1	1
sand	Fraction of soil which is sand	–	0.83	0.73
sfc	Volume of water at field capacity	$m^3\,m^{-3}$	0.143	0.143
silt	Fraction of soil that is silt	–	0.08	0.1
Soil fast	Fast soil carbon pool	$gC\,m^{-2}$	216	178
soilslow	Slow soil carbon pool	$gC\,m^{-2}$	432	4576
ssat	Volume of water at saturation	$m^3\,m^{-3}$	0.398	0.398
sucs	Suction at saturation	m	−0.106	−0.106
swilt	Volume of water at wilting	$m^3\,m^{-3}$	0.072	0.072

(*continued on next page*)

Table A1 (*continued*)

Parameter	Description	Units	Default	Site specific
tauleaf	Leaf transmittance	–	0.05	0.05
tauleafnir		–	0.25	0.25
tauwood		–	0.001	0.001
tauwoodnir		–	0.001	0.001
tvjmax		°C	15	15
tvjmin		°C	5	3
vbeta	Stomatal sensitivity to soil water	–	2	2
vcmax	Maximum RuBP carboxylation rate at top of leaf	$mol\ m^{-2}\ s^{-1}$	0.00006	0.0006
vegcf	Soil respiration scalar	–	8	8
vegheight	Vegetation height	m	20	7
WoodAI	Wood area index	$m^2\ m^{-2}$	1	1

A.2. Evapotranspiration package constants

Tables A.2 and A.3.

Table A2
Universal constants, which are kept constant (hard wired) for most conditions in the ET package for the used methods.

Constant	Description	Value	Unit
λ	Latent heat of vaporization	2.45	$MJ\ kg^{-1}$(at 20 °C)
δ	sigma Stefan–Boltzmann	4.903×10^{-9}	$MJ\ K^{-4}\ m^{-2}\ day^{-1}$
Gsc	Solar constant	0.0820	$MJ\ m^{-2}\ min^{-1}$
Roua	Mean density of air	1.2	$kg\ m^{-3}$ (at 20 °C)
Ca	Specific heat of air	0.001013	$MJ\ kg^{-1}\ K^{-1}$
G	Soil heat flux	Negligible for daily time step = 0 (Allen et al., 1998, page 68)	$W\ m^{-2}$
alphaA	Albedo for Class-A pan	0.14	–
α	Szilagyi–Jozsa formula	1.31 (Szilagyi and Jozsa, 2008)	–
	Brutsaert–Strickler formula	1.28 (Brutsaert and Strickler, 1979)	–
	GLEAM formulation	1.26 (Priestley and Taylor, 1972)	–
		0.97 for tall vegetation (*i.e.* trees)	

Table A3
Variable that can be changed for specific climate conditions in the ET package.

Variable	Description
Lat	Latitude
Lat_rad	Latitude in radians
as	Fraction of extra-terrestrial radiation reaching earth on sunless days
bs	Difference between fraction of extra-terrestrial radiation reaching full-sun days
Elev	Ground elevation above mean sea level (m)
z	Height of wind instrument (m)
a_0	Constant for estimating sunshine hours from cloud cover data
b_0	Constant for estimating sunshine hours from cloud cover data
c_0	Constant for estimating sunshine hours from cloud cover data
d_0	Constant for estimating sunshine hours from cloud cover data

A.3. GLEAM forcing datasets

Table A.4.

Table A4
Forcing datasets for GLEAM.

Variable	Forcing data	Data type	Version of GLEAM
Radiation	ERA-Interim	Reanalysis	v3a
	CERES L3SYN1DEG	Satellite	v3b, c
Precipitation	MSWEP v1.0	Merge	v3a
	TMPA 3B4 v7	Merge	v3b, c
Air temperature	ERA-Interim	Reanalysis	v3a
	AIRS L3RetStd v6.0	Satellite	v3b, c
Cover fractions	MOD44B v51	Satellite	v3a, b, c
Soil moisture	SMOS L3	Satellite	v3c
	ESA CCI v2.3	Satellite	v3a, b
	GLDAS Noah	Reanalysis	v3a, b, c
Soil properties	IGBP-DIS	Survey	v3a, b, c

A.4. Flux tower instruments and meteorological data

Table A.5, Fig. A.1.

Table A5
Flux tower instruments and measurements taken at Skukuza. The gas analyzer is calibrated on a quarterly basis.

Instrument	Measurement taken	Unit
Open path gas analyser (Li-cor Li7500)	Water vapor and carbon dioxide concentration	μmol mol^{-1}
Rain gage tipping bucket (Texas instruments)	Precipitation (0.246 mm resolution)	mm
Radiometer (Kipp and Zonnen CNR1)	Components of the radiation balance (*e.g.*, solar irradiance)	W m^{-2}
Air temperature sensor (RM Young)	Air temperature	°C
	Relative humidity	%
Three dimensional wind speed sensor (Campbell Scientific CSAT)	Wind velocity and wind direction	m s^{-1}
Two dimensional wind speed and direction (RM Young)		

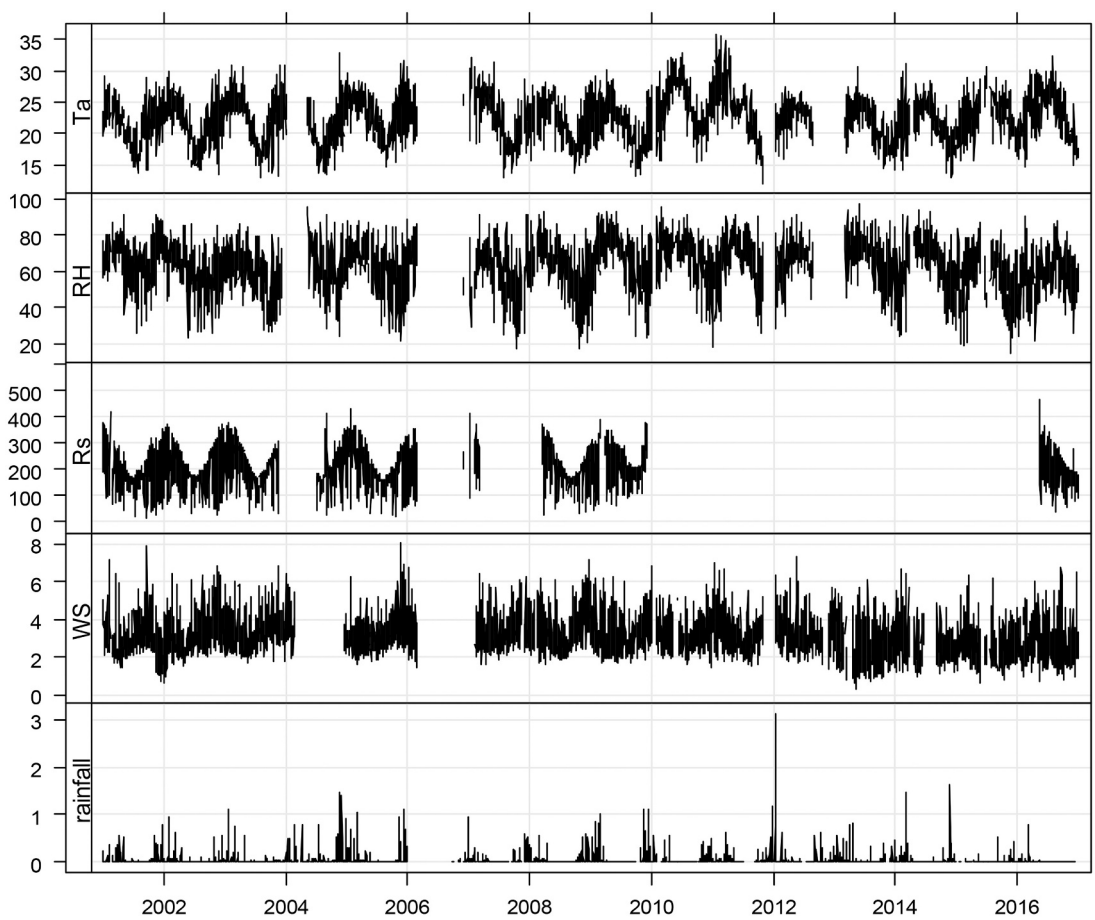

Fig. A1. Daily meteorological forcing data from the Skukuza flux tower used in the evapotranspiration models, air temperature (Ta, °C), relative humidity (RH, %), solar irradiance (Rs, W m^{-2}), wind speed (WS, m s^{-1}) and rainfall (mm day^{-1}).

A.5. Sensitivity of ET to meteorological variables

Figs. A2 and A.3

```
Call:
lm(formula = ET ~ Ta + RH + WS + Rs + SM, data = binded)

Residuals:
     Min       1Q   Median       3Q      Max 
-1.57604 -0.29970 -0.04436  0.48785  1.42272 

Coefficients:
             Estimate Std. Error t value Pr(>|t|)    
(Intercept)  0.072365   0.050024   1.447  0.14917    
Ta          -0.131835   0.026776  -4.924 1.48e-06 ***
RH           0.070203   0.007944   8.837  < 2e-16 ***
WS          -0.401655   0.146147  -2.748  0.00639 ** 
Rs          -0.008375   0.002081  -4.024 7.44e-05 ***
SM           0.179739   0.029397   6.114 3.39e-09 ***
---
Signif. codes:  0 ‘***’ 0.001 ‘**’ 0.01 ‘*’ 0.05 ‘.’ 0.1 ‘ ’ 1

Residual standard error: 0.6524 on 270 degrees of freedom
  (2028 observations deleted due to missingness)
Multiple R-squared:  0.5389,	Adjusted R-squared:  0.5303 
F-statistic: 63.11 on 5 and 270 DF,  p-value: < 2.2e-16
```

Fig. A2. Assessment of Sensitivity of ET to measured meteorological variables at Skukuza using multi-variate regression, with the significance codes: 0 ‘***’ 0.001 ‘**’ 0.01 ‘*’ 0.05 ‘.’ 0.1 ‘ ’ 1.

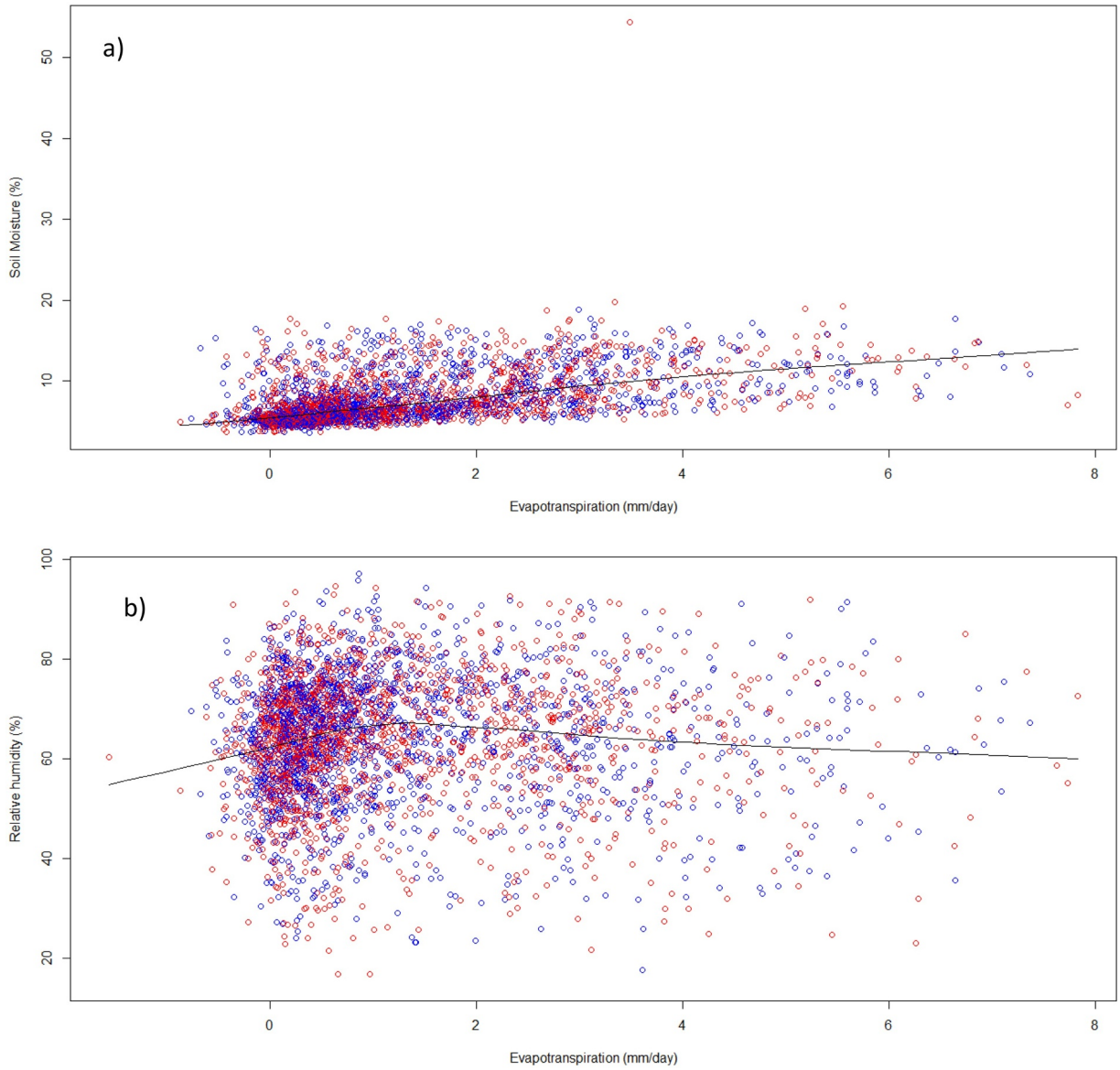

Fig. A3. Scatter plot showing agreement between ET, (a) soil moisture and (b) relative humidity.

A.6. Sensitivity of empirical models to alpha

Fig. A4.

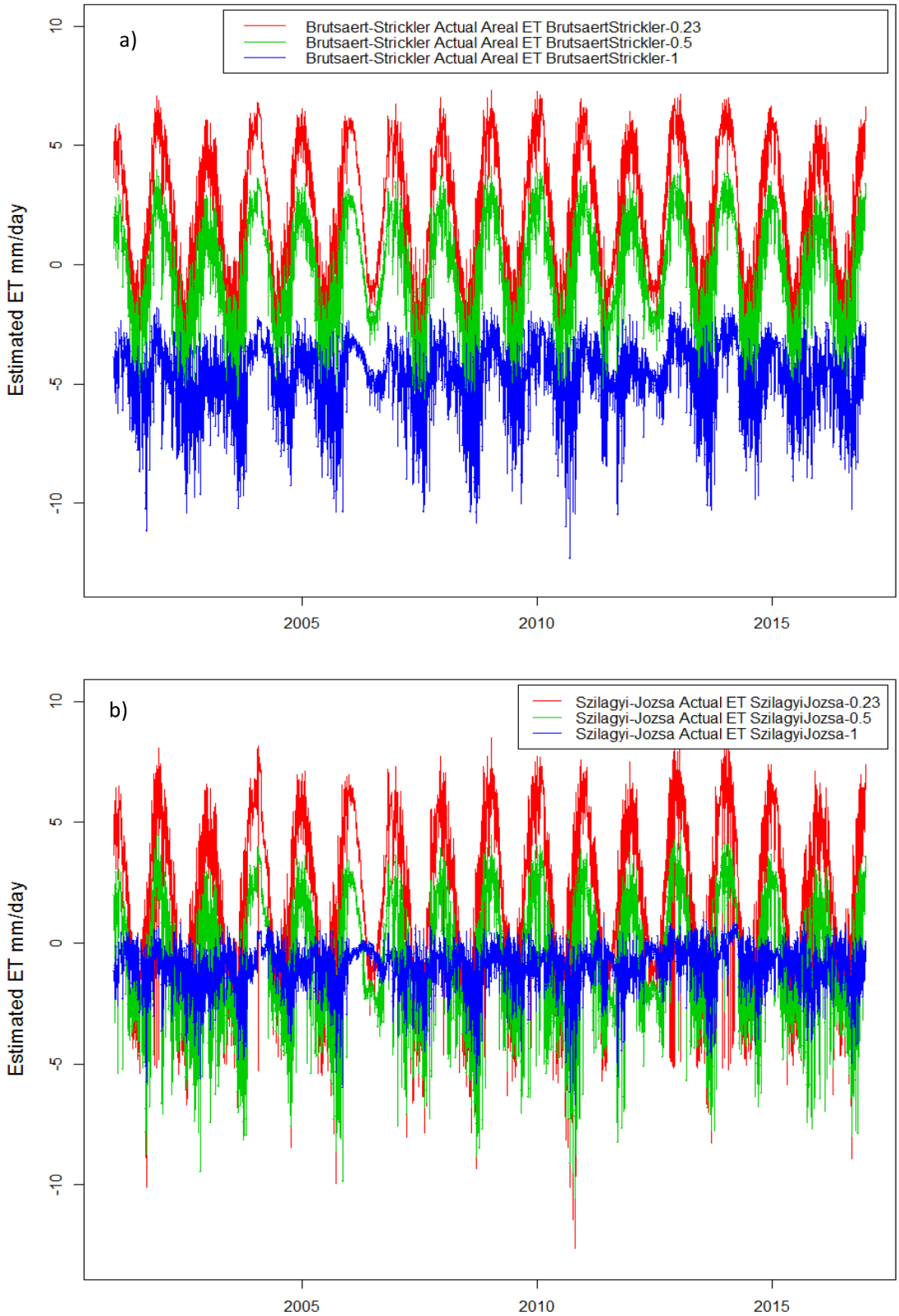

Fig. A4. Sensitivity of daily ET estimates from the; (a), Brutsaert–Strickler (b) Szilagyi–Jozsa and (c) Granger–Gray model to the alpha value as varied between 0.23 (red), 0.5 (green) and 1 (blue). (For interpretation of the references to color in this figure legend, the reader is referred to the web version of this article.)

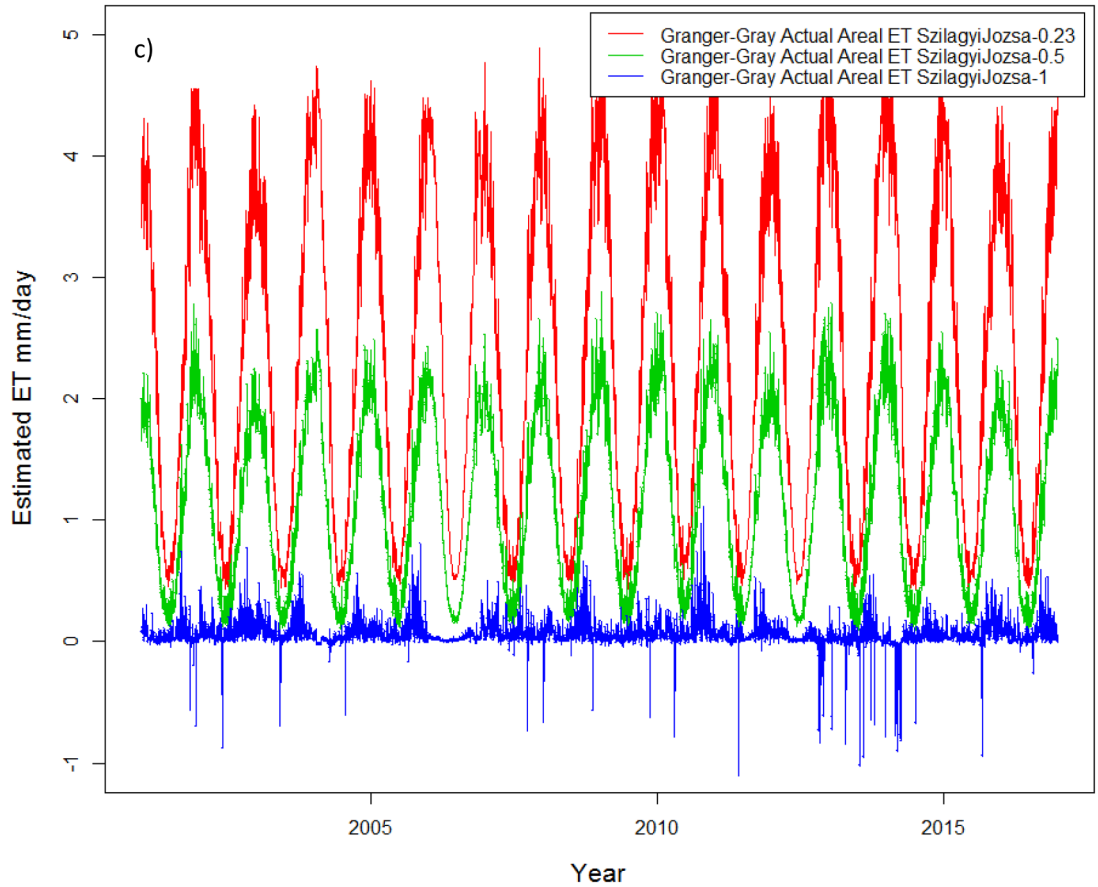

Fig. A4. (*continued*)

A.7. Descriptions of model parameters

Table A.6.

Table A6
Variables used in the computation of AET.

Variable	Description	Estimated-measured-constant	Unit
G_g	Evaporation parameter	$G_g = \frac{1}{0.798 + 0.20e^{4.902D_p}} + 0.006D_p$	–
D_p	Dimensionless relative drying power	$D_p = \frac{E_a}{E_a + \frac{R_n - G}{\lambda}}$	–
D	Vapor pressure deficit at the leaf surface		kPa
D_a	Vapor pressure deficit within the canopy		kPa
D_0	Fitted constant	1.5	kPa
a_1	Fitted constant	4.0	–
A	Assimilation rate	$A = C_i f(I)$, where $C_i$is the intercellular CO_2 concentration and $f(I)$is the function of incident light.	μmol m^{-2} s^{-1}
g_0	Fitted constant	0	mol $m^{-2}s^{-1}$
g_1	Fitted constant	3.37 $kPa^{0.5}$ for C3 and 1.10 $kPa^{0.5}$ for C4	mol m^{-2} s^{-1}
C_s	CO_2 concentration at the leaf surface	Measured	μmol mol^{-1}
β	Empirical soil moisture stress factor	$\beta = \frac{\theta - \theta_w}{\theta_{fc} - \theta_w}$	–
R_n	Net radiation	$R_n = R_{ns} - R_{nl}$	MJ kg^{-1}
R_{ns}	Net short incoming solar radiation	Measured	MJ kg^{-1}
R_{nl}	Net outgoing long solar radiation	Measured	MJ kg^{-1}
G	Soil/ground heat flux	Measured	MJ m^{-2} day^{-1}
λ	Latent heat of vaporization	2.45	MJ kg^{-1}(at 20°C)
γ	Psychometric constant	$\gamma = 0.00163\frac{p}{\lambda}$	kPa °C^{-1}
p	Atmospheric pressure	$p = 101.3(\frac{293 - 0.006Elev}{293})^{5.26}$	kPa
$Elev$	Elevation above sea level	Measured	m
E_a	Drying power of air	$E_a = f(u)(e_s - e_a)$	mm day^{-1}

(*continued on next page*)

Table A6 (*continued*)

Variable	Description	Estimated-measured-constant	Unit
e_s	Vapor pressure of air	$e_s = 0.6108 \exp[\frac{17.27 T_a}{T_a + 237.3}]$	kPa
e_a	Saturation vapor pressure	$e_a = \frac{e_s(T_{a\max}) + e_s(T_{a\min})}{2}$	kPa
w_c	Critical soil moisture		$m^3\ m^{-3}$
w_{wp}	Water retained below the wilting point		$m^3\ m^{-3}$
w_r	Soil moisture not available for root uptake		$m^3\ m^{-3}$
$w^{(w)}$	Soil moisture at the wettest layer		$m^3\ m^{-3}$
$w^{(l)}$	Surface soil moisture	$w_i^{(l)} = \frac{(F_{s,i}^{(l-1)} + F_{f,i}^{(l-1)} - E_{i-1}^{(l)} - F_{s,i}^{(l)})\Delta t}{\Delta z^{(l)}}$	$m^3\ m^{-3}$
$f(u)$	Priestley-Taylor wind function	$f(u) = 1.313 + 1.381 u_2$	–
u_2	Daily wind speed at 2 m	Measured	$m\ s^{-1}$
Δ	Slope of saturation vapor pressure	$\Delta = \frac{4098(0.6108 Exp(\frac{17.27 T_a}{T_a + 237.3}))}{(T_a + 237.3)^2}$	–
T_a	Mean daily air temperature	Measured	°C
E_{PT}	Wet environment evaporation	$E_{PT} = \alpha_{PT}[\frac{\Delta}{\Delta+\gamma}\frac{R_n}{\lambda} - \frac{G}{\lambda}]$; $\alpha_{PT} = 1.26$	$mm\ day^{-1}$
ET_p	PET	$ET_p = \frac{\Delta}{\Delta+\gamma}\frac{R_n}{\lambda} + \frac{\gamma}{\Delta+\gamma}E_a$	$mm\ day^{-1}$
E_i	Interception loss	Computed following Gash's model	$mm\ day^{-1}$
Γ	CO_2 compensation of assimilation in the presence of dark respiration	$\Gamma = \frac{\Delta}{\Delta+\gamma}$	μbar
r_s	Aerodynamic resistance from soil to canopy	$r_s = \ln\frac{z_{ref}}{z_0}\frac{\exp(2c_{SW}\Lambda) - \exp(2c_{SW}\Lambda(1-\frac{d}{h}))}{a_3^2 f_{sp}(\Lambda)c_{TL}2c_{SW}\Lambda}$	$s\ m^{-1}$
δq_d	Humidity deficit of air	$\delta q_d = \frac{1-RH}{100}$ RH is the relative humidity (%)	%
ρ_a	Air density	$\rho_a = \frac{p}{R * T_a}$	$kg\ m^{-3}$
p	Pressure	Measured	Pa
R	Specific gas constant for dry air	287.05	$J/(kg\ m^{-3})$
E_{sl}	Soil evaporation	$\lambda E_{sl} = \Gamma(R_n - G) + (1-\Gamma)\rho\lambda\delta q_d/r_s$	mm
E_{sp}	Potential evaporation	$\lambda E_{sp} = \lambda\rho(q^*(T_s) - q_{ref})/r_s$	mm
c_p	Specific heat capacity	$c_p = \lambda\gamma$	$J\ kg^{-1}\ °C^{-1}$
$G_{h,\ i}$	Heat conductance	$G_{w,i}^{-1} = G_{a,i}^{-1} + (nb_{bh}G_{b,i}^{-1})^{-1}$	–
$G_{w,\ i}$	Water conductance	$G_{w,i}^{-1} = G_{a,i}^{-1} + G_{b,i}^{-1} + G_{st,i}^{-1}$	–
$G_{r,\ i}$	Radiation conductance	$G_{r,i} = 4\varepsilon f\sigma_b T_a^3/c_p$	–
z	Height	Measured	m
VOD	Vegetation Optical Depth	Measured by satellite	–
S	Evaporative stress (Tall vegetation)	$S = 1 - (\frac{w_c - w_w}{w_c - w_{wp}})^2$	
	Evaporative stress (Short vegetation)	$S = \frac{1 - \sqrt{\frac{w_c - w_w}{w_c - w_{wp}}} + \frac{\tau}{0.8}}{2}$	–
	Evaporative stress (Bare soil)	$S = 1 - \sqrt{\frac{w_c - w_w}{w_c - w_{wp}}}$	–

References

Abd el-wahed, M.H., Snyder, R.L., 2015. Calculating sunshine hours and reference evapotranspiration in arid regions when solar radiation data are limited. Irrig. Drain. 64, 419–425. https://doi.org/10.1002/ird.1920.

Abramowitz, G., 2005. Towards a benchmark for land surface models. Geophys. Res. Lett. 32, 1–4. https://doi.org/10.1029/2005GL024419.

Abramowitz, G., Leuning, R., Clark, M., Pitman, A., 2008. Evaluating the performance of land surface models. J. Clim. 21, 5468–5481. https://doi.org/10.1175/2008JCLI2378.1.

Ahooghalandari, M., Khiadani, M., Jahromi, M.E., 2016. Developing equations for estimating reference evapotranspiration in Australia. Water Resour. Manag. 30, 3815–3828. https://doi.org/10.1007/s11269-016-1386-7.

Allen, R.G., Pereira, L.S., Raes, D., Smith, M., 1998. Crop evapotranspiration: guidelines fo computing crop water requirements. Irrig. Drainage Pap. 56, 300.

Archibald, S.A., Kirton, A., van der Merwe, M.R., Scholes, R.J., Williams, C.A., Hanan, N., 2009. Drivers of inter-annual variability in net ecosystem exchange in a semi-arid savanna ecosystem, South Africa. Biogeosciences 6, 251–266. https://doi.org/10.5194/bg-6-251-2009.

Bonan, G.B., 2008. Ecological climatology: concepts and applications, 2nd edition. Geogr. Res. 48, 221–222. https://doi.org/10.1111/j.1745-5871.2009.00640.x.

Bormann, H., 2011. Sensitivity analysis of 18 different potential evapotranspiration models to observed climatic change at German climate stations. Clim. Change 104, 729–753. https://doi.org/10.1007/s10584-010-9869-7.

Bouchet, R.J., 1963. Actual and potential evapotranspiration climatic significance. Int. Assoc. Sci. Hydrol. 62, 134–162. https://doi.org/10.1016/0022-1694(89)90249-7.

Brown, P., 2014. Basics of evaporation and evapotranspiration [WWW document]. URLhttp://extension.arizona.edu/sites/extension.arizona.edu/files/pubs/az1194.pdf(accessed 12.3.15).

Brutsaert, W., Stricker, H., 1979. An advection-aridity approach to estimate actual regional evapotranspiration. Water Resour. Res. 15, 443–450. https://doi.org/10.1029/WR015i002p00443.

Cai, J., Liu, Y., Lei, T., Santos, L., 2007. Estimating reference evapotranspiration with the Fao Penman – Monteith equation using daily weather forecast messages. Agric. For. Meteorol. 145, 22–35. https://doi.org/10.1016/j.agrformet.2007.04.012.

Cao, L., Bala, G., Caldeira, K., Nemani, R., Ban-Weiss, G., 2010. Importance of carbon dioxide physiological forcing to future climate change. Proc. Natl. Acad. Sci. https://doi.org/10.1073/pnas.0913000107.

Cowan, I.R., Farquhar, G.D., 1977. Stomatal function in relation to leaf metabolism and environment. Symp. Soc. Exp. Biol. 31, 471–505 doi:0081-1386.

De Kauwe, M.G., Kala, J., Lin, Y.S., Pitman, A.J., Medlyn, B.E., Duursma, R.A., Abramowitz, G., Wang, Y.P., Miralles, D.G., 2015. A test of an optimal stomatal conductance scheme within the CABLE land surface model. Geosci. Model Dev. 8, 431–452. https://doi.org/10.5194/gmd-8-431-2015.

Ding, R., Kang, S., Zhang, Y., Hao, X., Tong, L., 2013. Partitioning evapotranspiration into soil evaporation and transpiration using a modified dual crop coefficient model in irrigated maize field with ground-mulching. Agric. Water Manag. 127, 85–96. https://doi.org/10.1016/j.agwat.2013.05.018.

Enders, C.K., 2003. Using the expectation maximization algorithm to estimate coefficient alpha for scales with item-level missing data. Psychol. Methods 8, 322–337. https://doi.org/10.1037/1082-989X.8.3.322.

Feig, G.T., Mamtimin, B., Meixner, F.X., 2009. Soil Biogenic Emissions of Nitric Oxide from Arid and Semi-Arid Ecosystems. Biogeosciences. der Johannes Gutenberg-Universität Mainzhttps://doi.org/10.5194/bg-5-1723-2008.

Fisher, J.B., Debiase, T.A., Qi, Y., Xu, M., Goldstein, A.H., 2005. Evapotranspiration models compared on a Sierra Nevada forest ecosystem. Environ. Model. Softw. 20, 783–796. https://doi.org/10.1016/j.envsoft.2004.04.009.

Granger, R.J., 1998. Partitioning of energy during the snow-free season at the Wolf Creek

Research Basin. Wolf Creek Res. Basin Hydrol. Ecol. Environ. 33–44.
Granger, R.J., Gray, D.M., 1989. Evaporation from natural non saturated surfaces. J. Hydrol. 111, 21–29. https://doi.org/10.1016/0022-1694(89)90249-7.
Guo, D., Westra, S., Maier, H.R., 2016. An R package for modeling actual, potential and reference evapotranspiration. Environ. Model. Softw. 78, 216–224. https://doi.org/10.1016/j.envsoft.2015.12.019.
Haughton, N., Abramowitz, G., De Kauwe, M.G., Pitman, A.J., 2018. Does predictability of fluxes vary between FLUXNET sites? Biogeosciences 15, 4495–4513. https://doi.org/10.5194/bg-15-4495-2018.
Haughton, N., Abramowitz, G., Pitman, A.J., Or, D., Best, M.J., Johnson, H.R., Balsamo, G., Boone, A., Cuntz, M., Decharme, B., Dirmeyer, P.A., Dong, J., Ek, M., Guo, Z., Haverd, V., van den Hurk, B.J.J., Nearing, G.S., Pak, B., Santanello, J.A., Stevens, L.E., Vuichard, N., 2016. The plumbing of land surface models: is poor performance a result of methodology or data quality? J. Hydrometeorol. 17, 1705–1723. https://doi.org/10.1175/JHM-D-15-0171.1.
Högy, P., Wizemann, H.-.D., Eshonkulov, R., Ingwersen, J., Kremer, P., Streck, T., Weber, T.K.D., Pulatov, A., Poyda, A., 2019. Evaluating multi-year, multi-site data on the energy balance closure of eddy-covariance flux measurements at cropland sites in southwestern Germany. Biogeosciences 16, 521–540. https://doi.org/10.5194/bg-16-521-2019.
Jovanovic, N., Garcia, C.L., Bugan, R.D.H., Teich, I., Rodriguez, C.M.G., 2014. Validation of remotely-sensed evapotranspiration and NDWI using ground measurements at Riverlands, South Africa. Water SA 40, 211–220. https://doi.org/10.4314/wsa.v40i2.3.
Jovanovic, N., Mu, Q., Bugan, R.D.H., Zhao, M., 2015. Dynamics of Modis evapotranspiration in South Africa. Water SA 41, 79–91. https://doi.org/10.4314/wsa.v41i1.11.
Kottek, M., Grieser, J., Beck, C., Rudolf, B., Rubel, F., 2006. World map of the Köppen–Geiger climate classification updated. Meteorol. Zeitschrift. https://doi.org/10.1127/0941-2948/2006/0130.
Kowalczyk, E.A., Stevens, L., Law, R.M., Dix, M., Wang, Y.P., Harman, I.N., Haynes, K., Srbinovsky, J., Pak, B., Ziehn, T., 2013. The land surface model component of ACCESS: description and impact on the simulated surface climatology. Aust. Meteorol. Oceanogr. J. 63, 65–82. https://doi.org/10.22499/2.6301.005.
Kowalczyk, E.A., Wang, Y.P., Law, R.M., 2006a. The CSIRO atmosphere biosphere land exchange (CABLE) model for use in climate models and as an offline model. CSIRO Mar. Atmos. Res. Pap. 13, 1–42 doi:1921232390.
Kowalczyk, E.A., Wang, Y.P., Law, R.M., Davies, H.L., McGregor, J.L., Abramowitz, G., 2006. The CSIRO Atmosphere Biosphere Land Exchange (CABLE) model for use in climate models and as an offline model. doi:1921232390.
Law, R.M., Raupach, M.R., Abramowitz, G., Dharssi, I., Haverd, V., Pitman, A.J., Renzullo, L., Van Dijik, A., Wang, Y.-.P., 2012. The Commmunity Atmosphere Biosphere Land Exchange (CABLE) model road map for 2012-2017.
Leuning, R., 1995. A critical appraisal of a combined stomatal-photosynthesis model for C3 plants. Plant. Cell Environ. https://doi.org/10.1111/j.1365-3040.1995.tb00370.x.
Lu, J., Sun, G., McNulty, S.G., Amatya, D.M., 2005. A comparison of six potential evapotranspiration methods for regional use in the south eastern United States. J. Am. Water Resour. Assoc. 41, 621–633. https://doi.org/10.1111/j.1752-1688.2005.tb03759.x.
Majozi, N.P., Mannaerts, C.M., Ramoelo, A., Mathieu, R., Nickless, A., Verhoef, W., 2017. Analysing surface energy balance closure and partitioning over a semi-arid savanna FLUXNET site in Skukuza, Kruger National Park, South Africa. Hydrol. Earth Syst. Sci. 21, 3401–3415. https://doi.org/10.5194/hess-21-3401-2017.
Martens, B., Miralles, D.G., Lievens, H., Van Der Schalie, R., De Jeu, R.A.M.M., Fernández-Prieto, D., Beck, H.E., Dorigo, W.A., Verhoest, N.E.C.C., Férnandez-Prieto, D., Beck, H.E., Dorigo, W.A., Verhoest, N.E.C.C., 2017. GLEAM v3: satellite-based land evaporation and root-zone soil moisture. Geosci. Model Dev. Discuss. 10, 1903–1925. https://doi.org/10.5194/gmd-10-1903-2017.
Masih, I., Maskey, S., Mussá, F.E.F., Trambauer, P., 2014. A review of droughts on the African continent: a geospatial and long-term perspective. Hydrol. Earth Syst. Sci. 18, 3635–3649. https://doi.org/10.5194/hess-18-3635-2014.
McMahon, T.A., Peel, M.C., Lowe, L., Srikanthan, R., McVicar, T.R., 2013. Estimating actual, potential, reference crop and pan evaporation using standard meteorological data: a pragmatic synthesis. Hydrol. Earth Syst. Sci. 17, 1331–1363. https://doi.org/10.5194/hess-17-1331-2013.
Medlyn, B.E., Duursma, R.A., Eamus, D., Ellsworth, D.S., Prentice, I.C., Barton, C.V.M., Crous, K.Y., De Angelis, P., Freeman, M., Wingate, L., 2011. Reconciling the optimal and empirical approaches to modeling stomatal conductance. Glob. Chang. Biol. 17, 2134–2144. https://doi.org/10.1111/j.1365-2486.2010.02375.x.
Miralles, D.G., Gash, J.H., Holmes, T.R.H., De Jeu, R.A.M., Dolman, A.J., 2010. Global canopy interception from satellite observations. J. Geophys. Res. Atmos. 115, 1–8. https://doi.org/10.1029/2009JD013530.
Miralles, D.G., Holmes, T.R.H., De Jeu, R.A.M., Gash, J.H., Meesters, A.G.C.A., Dolman, A.J., 2011. Global land-surface evaporation estimated from satellite-based observations. Hydrol. Earth Syst. Sci. 15, 453–469. https://doi.org/10.5194/hess-15-453-2011.
Narapusetty, B., Delsole, T., Tippett, M.K., 2009. Optimal estimation of the climatological mean. J. Clim. https://doi.org/10.1175/2009JCLI2944.1.
Oxford, T., 2017. Understanding Climate Effects. Mail Guard [WWW Document]URL. https://mg.co.za/article/2017-02-10-00-understanding-climate-effects (accessed 3.14.17).
Palmer, A.R., Weideman, C., Finca, A., Everson, C.S., Hanan, N., Ellery, W., 2015. Modeling annual evapotranspiration in a semi-arid, African savanna: functional convergence theory, Modis Lai and the Penman–Monteith equation. African J. Range Forage Sci. 32, 33–39. https://doi.org/10.2989/10220119.2014.931305.
Penman, H.L., 1948. Natural evaporation from open water, bare soil and grass. In: Proceedings of the Royal Society of London. Series A, Mathematical and Physical Sciences. The Royal Society, pp. 120–145. https://doi.org/10.1017/CBO9781107415324.004.
Pereira, L.S., Allen, R.G., Smith, M., Raes, D., 2015. Crop evapotranspiration estimation with FAO56: past and future. Agric. Water Manag. 147, 4–20. https://doi.org/10.1016/j.agwat.2014.07.031.
Priestley, C.H.B., Taylor, R.J., 1972. On the assessment of surface heat flux and evaporation using large-scale parameters. Mon. Weather Rev. 100, 81–92. doi:10.1175/1520-0493(1972)100<0081:OTAOSH>2.3.CO;2.
Ramoelo, A., Majozi, N., Mathieu, R., Jovanovic, N., Nickless, A., Dzikiti, S., 2014. Validation of global evapotranspiration product (MOD16) using flux tower data in the African savanna, South Africa. Remote Sens. 6, 7406–7423. https://doi.org/10.3390/rs6087406.
Ratnam, J., Bond, W.J., Fensham, R.J., Hoffmann, W.A., Archibald, S., Lehmann, C.E.R., Anderson, M.T., Higgins, S.I., Sankaran, M., 2011. When is a "forest" a savanna, and why does it matter? Glob. Ecol. Biogeogr. 20, 653–660. https://doi.org/10.1111/j.1466-8238.2010.00634.x.
Scholes, R.J., Gureja, N., Giannecchinni, M., Dovie, D., Wilson, B., Davidson, N., Piggott, K., McLoughlin, C., Van der Velde, K., Freeman, A., Bradley, S., Smart, R., Ndala, S., 2001. The environment and vegetation of the flux measurement site near Skukuza, Kruger National Park. Koedoe 44, 73–84. https://doi.org/10.4102/koedoe.v44i1.187.
Shi, T.T., Guan, D.X., Wu, J.B., Wang, A.Z., Jin, C.J., Han, S.J., 2008. Comparison of methods for estimating evapotranspiration rate of dry forest canopy: eddy covariance, Bowen ratio energy balance, and Penman–Monteith equation. J. Geophys. Res. Atmos. 113, 1–15. https://doi.org/10.1029/2008JD010174.
Sun, Z., Gebremichael, M., Ardö, J., Nickless, A., Caquet, B., Merboldh, L., Kutschi, W., 2012. Estimation of daily evapotranspiration over Africa using MODIS/Terra and SEVIRI/MSG data. Atmos. Res. 112, 35–44. https://doi.org/10.1016/j.atmosres.2012.04.005.
Swemmer, A.M., Bond, W.J., Donaldson, J., Hempson, G.P., Malherbe, J., Smit, I.P.J., 2018. The ecology of drought – a workshop report. S. Afr. J. Sci. 114, 9–11. https://doi.org/10.17159/sajs.2018/5098.
Szilagyi, J., 2007. On the inherent asymmetric nature of the complementary relationship of evaporation. Geophys. Res. Lett. 34, 1–6. https://doi.org/10.1029/2006GL028708.
Szilagyi, J., Jozsa, J., 2008. New findings about the complementary relationship-based evaporation estimation methods. J. Hydrol. 354, 171–186. https://doi.org/10.1016/j.jhydrol.2008.03.008.
Tabari, H., Hosseinzadehtalaei, P., Willems, P., Martinez, C., 2016. Validation and calibration of solar radiation equations for estimating daily reference evapotranspiration at cool semi-arid and arid locations. Hydrol. Sci. J. 61, 610–619. https://doi.org/10.1080/02626667.2014.947293.
Taylor, K.E., 2001. Summarizing multiple aspects of model performance in a single diagram. J. Geophys. Res. 106, 7183–7192. https://doi.org/10.1029/2000JD900719.
Ukkola, A.M., Haughton, N., De Kauwe, M.G., Abramowitz, G., Pitman, A.J., 2017. FluxnetLSM R package (v1.0): a community tool for processing FLUXNET data for use in land surface modeling. Geosci. Model Dev. Discuss. 1–21. https://doi.org/10.5194/gmd-2017-58.
Valipour, M., 2014. Importance of solar radiation, temperature, relative humidity, and wind speed for calculation of reference evapotranspiration. Arch. Agron. Soil Sci. 0340, 1–17. https://doi.org/10.1080/03650340.2014.925107.
Wang, K., Dickinson, R.E., Wild, M., Liang, S., 2010a. Evidence for decadal variation in global terrestrial evapotranspiration between 1982 and 2002: 2. Results. J. Geophys. Res. Atmos. 115, 1–10. https://doi.org/10.1029/2010JD013847.
Wang, K., Dickinson, R.E., Wild, M., Liang, S., 2010b. Evidence for decadal variation in global terrestrial evapotranspiration between 1982 and 2002: 1. Model development. J. Geophys. Res. Atmos. 115, 1–11. https://doi.org/10.1029/2010JD013847.
Whitley, R., Beringer, J., Hutley, L.B., Abramowitz, G., De Kauwe, M.G., Evans, B., Haverd, V., Li, L., Moore, C., Ryu, Y., Scheiter, S., Schymanski, S.J., Smith, B., Wang, Y.-.P., Williams, M., Yu, Q., 2017. Challenges and opportunities in land surface modeling of savanna ecosystems. Biogeosciences 14, 4711–4732. https://doi.org/10.5194/bg-14-4711-2017.
Wilson, K.B., Hanson, P.J., Mulholland, P.J., Baldocchi, D.D., Wullschleger, S.D., 2000. A comparison of methods for determining forest evapotranspiration and its components: sap-flow, soil water budget, eddy covariance and catchment water balance. Agric. For. Meteorol. 106, 153–168. https://doi.org/10.1016/S0168-1923(00)00199-4.
Xu, C.Y., Chen, D., 2005. Comparison of seven models for estimation of evapotranspiration and groundwater recharge using lysimeter measurement data in Germany. Hydrol. Process. 19, 3717–3734. https://doi.org/10.1002/hyp.5853.
Xu, C.Y., Singh, V.P., 2005. Evaluation of three complementary relationship evapotranspiration models by water balance approach to estimate actual regional evapotranspiration in different climatic regions. J. Hydrol. 308, 105–121. https://doi.org/10.1016/j.jhydrol.2004.10.024.
Zhang, L., Dawes, W.R., Walker, G.R., 2001. Response of mean annual evapotranspiration to vegetation changes at catchment scale. Water Resour. Res. 37, 701–708. https://doi.org/10.1029/2000WR900325.
Zhang, Y., Zheng, H., Chiew, F.H.S., Arancibia, J.P., Zhou, X., 2016. Evaluating regional and global hydrological models against streamflow and evapotranspiration measurements. J. Hydrometeorol. 17, 995–1010. https://doi.org/10.1175/JHM-D-15-0107.1.